Chemical Physics 128 (1988) 99–123
North-Holland, Amsterdam

QUANTUM TRANSPORT AND LOCALIZATION IN DISORDERED MEDIA: LIOUVILLE SPACE DYNAMICS WITH FREQUENCY-DEPENDENT DEPHASING

Shaul MUKAMEL [1], Daniel S. FRANCHI and Roger F. LORING [2]
Department of Chemistry, University of Rochester, Rochester, NY 14627, USA

Received 18 December 1987

A unified theory of quantum transport processes and spectral lineshapes in condensed phases in terms of frequency-dependent dephasing rates is developed. The effective dephasing approximation (EDA) provides a self-consistent procedure for calculating the transport properties of a quantum particle in a disordered medium. It is based on mapping the averaged Liouville space propagator into the propagator of a particle moving in an ordered lattice with an effective frequency-dependent dephasing rate. The effective dephasing rate is determined self-consistently. The Liouville equation for the averaged density matrix is isomorphic to a linearized Boltzmann equation, and the effective dephasing rate represents a generalized BGK strong-collision operator. Applications of the EDA to the Anderson model of static disorder and to a model of dynamical disorder with a finite timescale are presented, and are shown to be in agreement with scaling theories. The frequency-dependent dephasing which determines the transport processes is found to be much more sensitive to quantum localization than the dephasing which enters into the calculation of optical lineshapes and densities of states.

1. Introduction

Dephasing processes play an important role in controlling the optical properties of matter. The width of spectral lineshapes is often dominated by the loss of phase among the optically active levels, and the interpretation of linear and nonlinear optical measurements depends heavily on the understanding of the underlying dephasing mechanism [1,2]. The concept of dephasing is not restricted, however, to spectroscopy. Any complex dynamics involving many degrees of freedom requires a *reduced description* whereby we follow explicitly only a small set of dynamical variables and the effects of the other degrees of freedom result in dephasing and relaxation. We have recently developed a theory of rate processes (e.g., electron transfer) in condensed phases which is based on the analogy with the problem of spectral lineshapes and interprets the dynamics of solvation in terms of dephasing [3]. Similarly transport processes in condensed phases (the Anderson model [4–6], the polaron problem [7]) may also be conveniently interpreted in terms of properly defined dephasing processes. The effective dephasing approximation (EDA) yields a self-consistent mode-coupling equation in Liouville space that provides a simple and systematic method to calculate transport properties of a quantum particle in a disordered medium [8–11]. In the EDA, the Liouville equation for the ensemble-averaged density matrix is mapped onto the equation of motion of a particle whose dynamics are characterized by a frequency-dependent dephasing rate $\Gamma(\epsilon)$. $\Gamma(\epsilon)$ is determined self-consistently. The transport properties at long times are determined by the behavior of $\Gamma(\epsilon)$ for small ϵ. If $\Gamma=0$, the particle undergoes coherent motion on an ordered lattice. In this limit, the system is characterized by extended Bloch states. If Γ is large but finite, the motion is diffusive (incoherent) and can be described by a Pauli master equation. If $\Gamma(\epsilon)$ has an infrared divergence, $\Gamma(\epsilon) \propto \epsilon^{-1}$, the particle is localized. The signature of the localization (metal–nonmetal) transition is the crossover from a dephasing rate that is finite at small frequencies to one that displays an infrared divergence. This approach provides a straight-

[1] Camille and Henry Dreyfus Teacher-Scholar.
[2] Present address: Department of Chemistry, Cornell University, Ithaca, NY 14853, USA.

forward way to calculate the transport properties of a particle or quasiparticle in a condensed phase medium, and to relate these properties to linear and nonlinear optical lineshapes. In section 2, we consider the absorption lineshape of a single absorber and introduce the frequency-dependent dephasing. In section 3, we show how intermolecular dephasing affects excitation transfer in dimers. The problem of excitation transport is considered in section 4 where we introduce and analyze the averaged Liouville equation with a frequency-dependent dephasing rate. In section 5, we show the connection between the effective dephasing introduced in section 4 and the BGK strong collision model within the Boltzmann equation. In section 6, we introduce and analyze the EDA for the Anderson model of static disorder. In section 7, we consider a model of dynamical disorder and compare the frequency-dependent dephasing for the absorption lineshape (intramolecular dephasing) and for the transport (intermolecular dephasing). The intermolecular dephasing is found to be much more sensitive to the localization transition than the intramolecular dephasing. We summarize our results in section 8.

2. Dephasing in single absorber spectra

In this section we introduce the concept of frequency-dependent dephasing by analyzing a simple model of spectral broadening in a dynamically disordered medium [1,2]. We consider a molecule with two electronic states, the ground state $|g\rangle$ with energy E_g and an excited state $|e\rangle$ with energy $E_g+\hbar\omega_{eg}$. The molecular Hamiltonian is

$$H=|g\rangle E_g\langle g|+|e\rangle(E_g+\hbar\omega_{eg}-i\hbar\gamma_e/2)\langle e|\,. \tag{2.1}$$

γ_e^{-1} is the lifetime of the excited state. For an isolated molecule, ω_{eg} is a constant. We shall assume, however, that due to the interaction with an external bath (e.g., phonons, solvent motions), ω_{eg} undergoes a time-dependent stochastic modulation, i.e.,

$$\omega_{eg}=\bar{\omega}_{eg}+\delta\omega_{eg}(t)\,, \tag{2.2}$$

where $\bar{\omega}_{eg}$ is the mean electronic energy gap. $\delta\omega_{eg}(t)$ is taken to be a stationary Gaussian Markovian process with zero mean [1,2,12–14]

$$\langle\delta\omega_{eg}(t)\rangle=0\,, \tag{2.3a}$$

and a correlation function

$$\langle\delta\omega_{eg}(t)\delta\omega_{eg}(0)\rangle=\Delta^2\exp(-\Lambda|t|)\,. \tag{2.3b}$$

Here $\langle\ldots\rangle$ denotes averaging over the stochastic variables. Δ denotes the magnitude of the fluctuations and Λ^{-1} is their time scale (correlation time). The averaged density matrix element representing the coherence between the ground and the excited states, $\hat{\rho}_{eg}(t)$, satisfies the equation

$$\langle\dot{\hat{\rho}}_{eg}(t)\rangle=-i\bar{\omega}_{eg}\langle\hat{\rho}_{eg}(t)\rangle-\int_0^t d\tau\exp[-i\bar{\omega}_{eg}(t-\tau)]\,\hat{\Gamma}(t-\tau)\,\langle\hat{\rho}_{eg}(\tau)\rangle\,. \tag{2.4}$$

The Laplace transform of any function of time $\hat{f}(t)$ is defined as

$$f(\epsilon)\equiv\int_0^\infty d\tau\exp(-\epsilon\tau)\hat{f}(\tau)\,,\quad \hat{f}=\hat{\rho}_{eg},\hat{J},\hat{\Gamma},\text{ etc.} \tag{2.5}$$

The solution of eq. (2.4) is

$$\langle\rho_{eg}(\epsilon)\rangle=J(\epsilon+i\bar{\omega}_{eg})\langle\hat{\rho}_{eg}(0)\rangle\,, \tag{2.6}$$

with

$$\hat{J}(\tau)=\exp[-g(\tau)]\,, \tag{2.7}$$

and

$$g(\tau)=\int_0^{\tau} d\tau_1 \int_0^{\tau_1} d\tau_2 \,\langle \delta\omega_{eg}(\tau_2)\delta\omega_{eg}(0)\rangle\,. \tag{2.8}$$

Upon the substitution of eqs. (2.3) in eq. (2.8) we get

$$g(\tau)=(\Delta^2/\Lambda^2)[\exp(-\Lambda\tau)-1+\Lambda\tau]\,. \tag{2.9}$$

Alternatively eq. (2.6) can be recast in the form

$$J(\epsilon)=\frac{1}{\epsilon+\Gamma(\epsilon)} \tag{2.10}$$

$$\Gamma(\epsilon)=\cfrac{\Delta^2}{\epsilon+\Lambda+\cfrac{2\Delta^2}{\epsilon+2\Lambda+\cfrac{3\Delta^2}{\epsilon+3\Lambda...}}}\,, \tag{2.11}$$

where $\Gamma(\epsilon)$ is a *frequency-dependent dephasing rate.* The absorption lineshape at frequency ω is given by [1,2,12–14]

$$\sigma(\omega)=(1/\pi)\,\mathrm{Re}\,J[\gamma_e/2-i(\omega-\bar{\omega}_{eg})]\,. \tag{2.12}$$

We next introduce the definitions

$$\Gamma[-i(\omega-\bar{\omega}_{eg})+\gamma_e/2]\equiv\Gamma'(\omega)-i\Gamma''(\omega)\,, \tag{2.13}$$

where Γ' and Γ'' represent the real and the imaginary parts of $\Gamma[-i(\omega-\bar{\omega}_{eg})+\gamma_e/2]$, respectively. Eq. (2.12) takes the form

$$\sigma(\omega)=\frac{[\Gamma'(\omega)+\gamma_e/2]/\pi}{[\omega-\bar{\omega}_{eg}+\Gamma''(\omega)]^2+[\Gamma'(\omega)+\gamma_e/2]^2}\,. \tag{2.14}$$

The absorption lineshape depends on the dimensionless parameter $\kappa=\Lambda/\Delta$. For $\kappa\gg 1$ the lineshape assumes a Lorentzian form and the line is homogeneously broadened whereas for $\kappa\ll 1$, the lineshape is inhomogeneous and assumes a Gaussian form. The full-width at half maximum (fwhm) of the lineshape is [12–14]

$$\delta=\frac{2.355+1.76\kappa}{1+0.85\kappa+0.88\kappa^2}\Delta\,. \tag{2.15}$$

$\Gamma(\epsilon)$ is displayed in fig. 1. We have varied κ by varying Δ and Λ keeping $\delta=1$. For $\kappa\gg 1$, $\Gamma(\epsilon)=\Delta^2/\Lambda$, whereas for $\kappa\ll 1$, we have

$$\Gamma(\epsilon)=[(\pi/2\Delta^2)^{1/2}\exp(\epsilon^2/2\Delta^2)\,\mathrm{erfc}(\epsilon/\sqrt{2}\Delta)]^{-1}-\epsilon\,. \tag{2.16}$$

Fig. 1 illustrates how $\Gamma(\epsilon)$ vanishes for $\epsilon\gg\Lambda$.

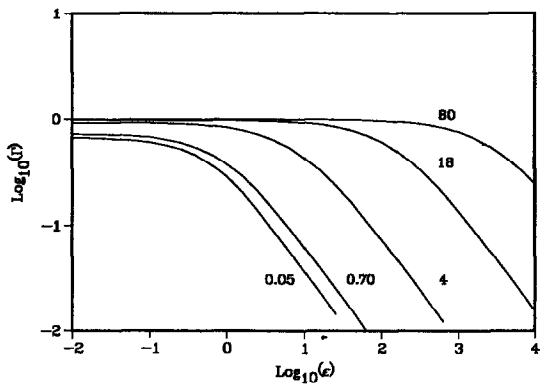

Fig. 1. The frequency-dependent dephasing rate $\Gamma(\epsilon)$ for a single molecule is calculated from eq. (2.11). Each curve is labeled by $\kappa \equiv \Lambda/\Delta$. Δ and Λ are varied keeping the fwhm of the absorption lineshape (eq. (2.15)) fixed at $\delta = 1$.

Another spectroscopic observable of interest is this system in the steady state dispersed emission when the system is subject to a monochromatic field with frequency ω. That emission consists of a broad fluorescence and a sharp Rayleigh (or Raman) component. We have recently shown [14] that the quantum yield of the Raman component is

$$Y_R(\omega) = \gamma_e / [\gamma_e + \Gamma'(\omega)] . \tag{2.17}$$

The vanishing of $\Gamma'(\omega)$ for large detuning ω makes this yield go to unity for large detunings. Fig. 1 implies that the variation of $\Gamma'(\omega)$ with ω occurs on an ω range corresponding to the typical bath time scale in the problem (Λ^{-1}).

3. The role of dephasing in excitation transfer in dimers

In the previous section, we introduced a stochastic model of dephasing for a single two-level molecule. For that system the relevant dynamical observables are the absorption and the emission lineshapes. In this section, we consider the simplest model of energy transfer involving two molecules. An excitation can reside on the first molecule (state $|1\rangle$) or on the second molecule (state $|2\rangle$). The two excited states are coupled by a matrix element $H_{12} = J$ allowing for excitation transfer. In addition the energy of each molecular excited state is undergoing independent fluctuations as given by eqs. (2.2) and (2.3). The equation of motion of the density matrix $\hat{\rho}$ for the dimer is

$$\partial\hat{\rho}/\partial t = [\mathbf{A} + \mathbf{B}\omega_{12}(t)]\hat{\rho} , \tag{3.1a}$$

with

$$\omega_{12}(t) \equiv \delta\omega_1(t) - \delta\omega_2(t) . \tag{3.1b}$$

Here $\delta\omega_1(t)$ ($\delta\omega_2(t)$) is $\delta\omega_{eg}(t)$ of state $|1\rangle$ ($|2\rangle$). Using eqs. (2.2) and (2.3), we get

$$\langle \omega_{12}(t)\omega_{12}(0)\rangle = 2\Delta^2 \exp(-\Lambda|t|) . \tag{3.1c}$$

The density matrix of the system has four elements which form a column vector whose components (from top to bottom) are taken to be: $\hat{\rho}_{11}, \hat{\rho}_{22}, \hat{\rho}_{12}$ and $\hat{\rho}_{21}$. Here $\hat{\rho}_{jj}$ represents the probability that the excitation resides at molecule j, and $\hat{\rho}_{jk}$ represents a coherence between molecules j and k. The operators $\mathbf{A}$ and $\mathbf{B}$ are represented by 4×4 matrices with elements $A_{ij,kl}$ and $B_{ij,kl}$, where $i, j, k, l = 1, 2$:

$$\mathbf{A}=\mathrm{i}J\begin{pmatrix} 0 & 0 & 1 & -1 \\ 0 & 0 & -1 & 1 \\ 1 & -1 & 0 & 0 \\ -1 & 1 & 0 & 0 \end{pmatrix}, \quad \mathbf{B}=\mathrm{i}\begin{pmatrix} 0 & 0 & 0 & 0 \\ 0 & 0 & 0 & 0 \\ 0 & 0 & 1 & 0 \\ 0 & 0 & 0 & -1 \end{pmatrix}. \tag{3.2}$$

The solution of eq. (3.1a), averaged over the stochastic fluctuations, is given by

$$\langle\hat{\rho}(t)\rangle=\hat{\mathbf{G}}(t)\hat{\rho}(0)\,. \tag{3.3}$$

Like the operators **A** and **B** in eq. (3.1), $\hat{\mathbf{G}}(t)$ is a 4×4 matrix. Eqs. (3.1a) and (3.1b) are identical with the equations of motion of a two-level system with Gaussian frequency modulation in an electromagnetic field of arbitrary intensity [15,16]. The equation of motion in that problem is identical with eq. (3.1a), if the Rabi frequency is replaced by $2J$, and the rate of population decay from level 2 to level 1 is set to zero. (The Rabi frequency is $\mu E/\hbar$, where μ is the transition dipole moment of the two-level system and E is the electric field amplitude.) $\mathbf{G}(\epsilon)$, the Laplace transform of $\hat{\mathbf{G}}(t)$, can be represented as a matrix continued fraction [9,15,16] and is given by

$$\mathbf{G}(\epsilon)=[\epsilon-\mathbf{A}-\boldsymbol{\gamma}(\epsilon)]^{-1}\,, \tag{3.4a}$$

$$\boldsymbol{\gamma}(\epsilon)=\cfrac{2\Delta^2}{\epsilon+\Lambda-\mathbf{A}-\mathbf{B}\cfrac{4\Delta^2}{\epsilon+2\Lambda-\mathbf{A}-\ldots}\mathbf{B}}\,. \tag{3.4b}$$

$\boldsymbol{\gamma}(\epsilon)$ represents a *frequency-dependent dephasing matrix*. It has only four nonzero matrix elements $\gamma_{12,12}$, $\gamma_{12,21}$, $\gamma_{21,12}$ and $\gamma_{21,21}$. We shall denote them Γ_1, Γ_2, Γ_3 and Γ_4, respectively. Note that Γ_1 and Γ_4 represent the damping of *intermolecular coherence*, whereas Γ_2 and Γ_4 represent transfer of intermolecular coherence (interchange of ρ_{12} and ρ_{21}). In contrast, $\Gamma(\epsilon)$ introduced in section 2 represents the dephasing of an *intramolecular optical coherence*. In the absence of dephasing ($\Delta=0$), eq. (3.4) represents a coherent evolution among the two states. In the fast modulation limit $\kappa\gg1$, we get

$$\gamma_{12,12}=\gamma_{21,21}=2\Delta^2/\Lambda\,, \quad \gamma_{12,21}=\gamma_{21,12}=0 \tag{3.5}$$

$\boldsymbol{\gamma}(\epsilon)$ is independent, in this case, of ϵ, and $\mathbf{G}(\epsilon)$ reduces to the Green function of the optical Bloch equations. If in addition $\gamma_{12,12}\gg J$, $\mathbf{G}(\epsilon)$ becomes the Green function solution to coupled rate equations (Pauli master equation) with a rate of excitation transfer between the molecules equal to $J^2/\gamma_{12,12}$.

In fig. 2, we display $\gamma_{12,12}$ and $\gamma_{12,21}$ for various values of κ, which is varied by changing Δ and Λ and keeping δ (eq. (2.15)) fixed. We have taken $J=1$ and $\delta=1.5\times10^5$. In figs. 3 and 4, we repeat these calculations for $\delta=1.5\times10^3$ and $\delta=0.15$, respectively.

Another quantity of interest is $\mathscr{P}_0(t)$, the probability for the excitation to remain at time t on molecule 1, when it was on molecule 1 at $t=0$. The Laplace transform of $\mathscr{P}_0(t)$ *is*

$$P_0(\epsilon)=\epsilon^{-1}-\tfrac{1}{2}[\epsilon^{-1}-G_{11,11}(\epsilon)]\,. \tag{3.6}$$

$\mathscr{P}_0(t)$ was calculated by inverting the Laplace transform (eq. (3.6)) numerically using the Stehfest algorithm [17]. In fig. 5, we display $\mathscr{P}_0(t)$. The various curves in fig. 5a were obtained by setting $J=1$, $\Lambda=0$ (infinite correlation time), and varying the fwhm δ. In fig. 5b, we repeat these calculations for the same values of δ but with a short correlation time, $\Lambda=100$. For small δ, the $\Lambda=0$ and $\Lambda=100$ curves are similar and represent almost coherent motion. As δ increases, the time evolution becomes substantially different reflecting the effects of the bath time scale Λ^{-1}.

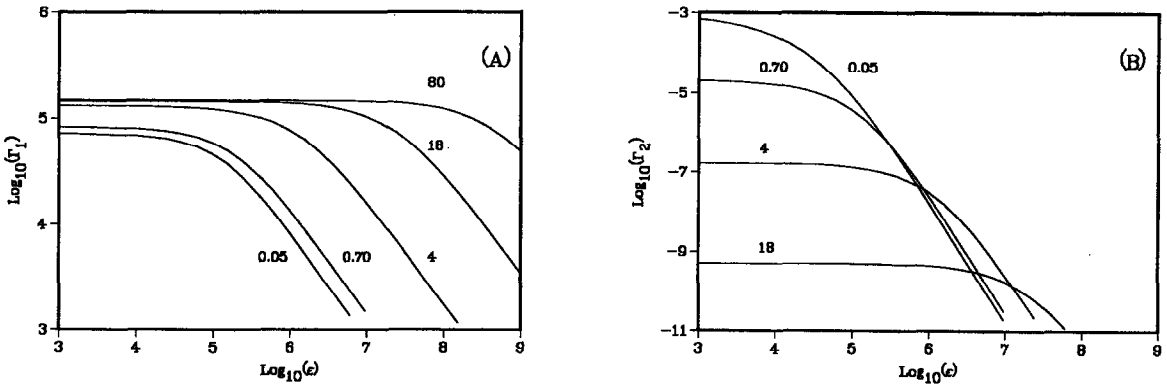

Fig. 2. (a) The diagonal element of the frequency-dependent dephasing matrix for the dimer $\Gamma_1 \equiv \gamma_{12,12}$ is calculated from eq. (3.4b). Each curve is labeled by $\kappa \equiv \Lambda/\Delta$. Δ and Λ are varied, keeping the fwhm of the absorption spectrum (eq. (2.15)) fixed at $\delta = 1.5 \times 10^5$. (b) The off-diagonal element of the frequency-dependent dephasing for the dimer $\Gamma_2 \equiv \gamma_{12,21}$ is calculated from eq. (3.4b). The other parameters are the same as in (a).

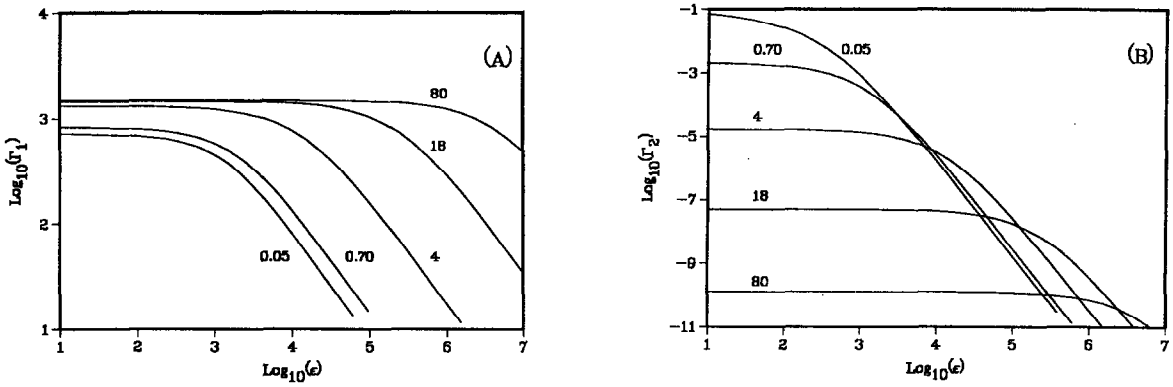

Fig. 3. (a) The same as fig. 2a, but with $\delta = 1.5 \times 10^3$. (b) The same as fig. 2b, but with $\delta = 1.5 \times 10^3$.

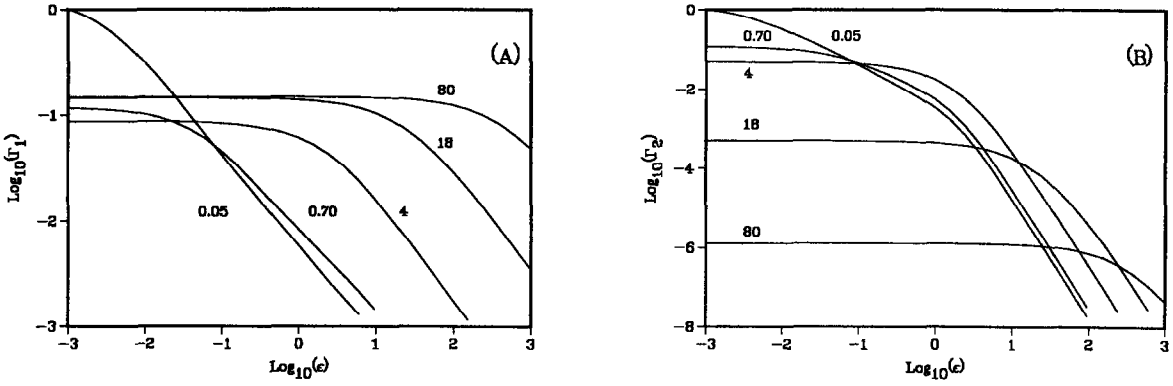

Fig. 4. (a) The same as fig. 2a, but with $\delta = 0.15$. (b) The same as fig. 2b, but with $\delta = 0.15$.

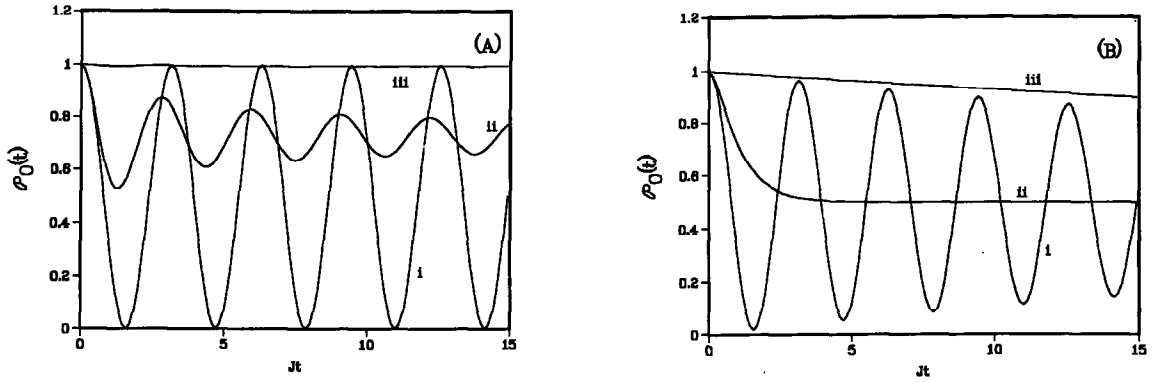

Fig. 5. (a) $\mathscr{P}_0(t)$, the probability for the excitation to remain at the origin at time t is shown for the dimer in the static limit ($\Delta=0$). The calculation was made using eq. (3.6): (i) $\Delta/2J=10^{-2}$, $\delta/2J=2.35\times10^{-2}$; (ii) $\Delta/2J=1$, $\delta/2J=2.35$; (iii) $\Delta/2J=100$, $\delta/2J=23.5$. For $\Delta\ll J$, the excitation moves coherently from site to site, and $\mathscr{P}_0(t)$ is oscillatory. As Δ is increased, the oscillations are damped, and their amplitude decreases. (b) $\mathscr{P}_0(t)$, the probability for the excitation to remain at the origin at time t is shown for the dimer for $\Delta/2J=100$. curves (i)–(iii) have the same values of δ as the corresponding curves in (a). (i) $\Delta/2J=1.08$, $\delta/2J=2.35\times10^{-2}$; (ii) $\Delta/2J=10.7$, $\delta/2J=2.35$; (iii) $\Delta/2J=136$, $\delta/2J=23.5$. The exciton moves coherently for small Δ, and $\mathscr{P}_0(t)$ displays oscillations. For large Δ, $\mathscr{P}_0(t)$ decays monotonically.

4. Excitation dynamics with a frequency-dependent effective dephasing rate

In this section we extend the notion of an intermolecular dephasing rate introduced in section 3 for a dimer, to excitation transport in an infinite lattice. We consider a quantum particle whose motion on a lattice is described by the tight-binding Hamiltonian

$$H=\sum_x E_x|x\rangle\langle x|+\sum_{x\neq x'}\hbar J(x-x')|x\rangle\langle x'|\,. \tag{4.1}$$

$|x\rangle$ denotes the state in which the particle is localized at the lattice point x. $J(x-x')$ is the transfer matrix element between sites and E_x is the particle energy at site x. The Hamiltonian (4.1) can contain various types of disorder. Both E_x and $J(x-x')$ can be randomly distributed with some specified statistical properties. In the Anderson model [4–6] of diagonal disorder, for example, $\{E_x\}$ are independent random variables with a distribution $R(E_x)$, and $J(x-x')$ is translationally invariant. The disorder can be static or dynamic in nature. In the latter case, E_x or $J(x-x')$ undergo random fluctuations. At this stage the precise nature of the disorder need not be specified. Specific models for disorder will be considered in sections 6 and 7. The density matrix of the excitation obeys the Liouville equation

$$\dot{\hat{\rho}}=-i\hbar^{-1}[H,\hat{\rho}]=-iL\hat{\rho}\,. \tag{4.2}$$

It is convenient to change variables from x and x' to r and s, which are defined by

$$x=r-s/2\,,\quad x'=r+s/2\,. \tag{4.3}$$

The density matrix element $\hat{\rho}(r,s,t)$ is defined by

$$\hat{\rho}(r,s,t)\equiv\langle r-s/2|\hat{\rho}|r+s/2\rangle\,. \tag{4.4}$$

$\hat{\rho}(r,0,t)$ is a diagonal element of the density matrix, and gives the probability that the excitation is located at position r at time t. For $s\neq0$, $\hat{\rho}(r,s,t)$ is a coherence that carries information on the phase relationship between two sites separated by a displacement s. Substitution of eq. (4.1) into eq. (4.2) yields the equation of motion of $\hat{\rho}(r,s,t)$:

$$\dot{\hat{\rho}}(\boldsymbol{r},\boldsymbol{s},t)=-\mathrm{i}\sum_{\boldsymbol{a}}J(\boldsymbol{a})[\hat{\rho}(\boldsymbol{r}+\boldsymbol{a}/2,\boldsymbol{s}-\boldsymbol{a},t)-\hat{\rho}(\boldsymbol{r}+\boldsymbol{a}/2,\boldsymbol{s}+\boldsymbol{a},t)]-\mathrm{i}\hbar^{-1}(E_{\boldsymbol{r}-\boldsymbol{s}/2}-E_{\boldsymbol{r}+\boldsymbol{s}/2})\hat{\rho}(\boldsymbol{r},\boldsymbol{s},t)\,. \tag{4.5}$$

The index $\boldsymbol{a}$ runs over all displacements in the lattice. Our goal is the calculation of the ensemble averaged density matrix $\hat{\sigma}(\boldsymbol{r},\boldsymbol{s},t)$:

$$\hat{\sigma}(\boldsymbol{r},\boldsymbol{s},t)\equiv\langle\hat{\rho}(\boldsymbol{r},\boldsymbol{s},t)\rangle\,. \tag{4.6}$$

The angular brackets in eq. (4.6) represent an average over any random variables (E or J) in the model. We introduce the following *ansatz* for the form of the reduced equation of motion of $\hat{\sigma}(\boldsymbol{r},\boldsymbol{s},t)$ [8–11]:

$$\dot{\hat{\sigma}}(\boldsymbol{r},\boldsymbol{s},t)=-\mathrm{i}\sum_{\boldsymbol{a}}\langle J(\boldsymbol{a})\rangle[\hat{\sigma}(\boldsymbol{r}+\boldsymbol{a}/2,\boldsymbol{s}-\boldsymbol{a},t)-\hat{\sigma}(\boldsymbol{r}+\boldsymbol{a}/2,\boldsymbol{s}+\boldsymbol{a},t)]$$

$$-\int_0^t\mathrm{d}\tau\,\hat{\Gamma}(t-\tau)[\hat{\sigma}(\boldsymbol{r},\boldsymbol{s},\tau)-f(\boldsymbol{s})\hat{\sigma}(\boldsymbol{r},0,\tau)]\,. \tag{4.7}$$

The first term in eq. (4.7) describes motion on a translationally invariant lattice. The second term contains two functions which remain to be specified, $\hat{\Gamma}(t)$ and $f(\boldsymbol{s})$. If we choose $\hat{\Gamma}(t)$ to decay rapidly on all relevant time scales, $\hat{\Gamma}(t)=\gamma\delta(t)$, and choose $f(\boldsymbol{s})=\delta_{\boldsymbol{s},0}$, then eq. (4.7) reduces to the Haken–Strobl equation of motion for the density matrix of an exciton in a molecular crystal [18]. For this choice of $\hat{\Gamma}(t)$ and $f(\boldsymbol{s})$, the second term in eq. (4.7) causes all coherences $\hat{\sigma}(\boldsymbol{r},\boldsymbol{s},t)$ for $\boldsymbol{s}\neq0$ to decay with a dephasing rate γ. Thus $\hat{\Gamma}(t)$ can be viewed as a generalized time-dependent dephasing rate.

We next turn to the calculation of the density matrix $\hat{\sigma}$, which can be determined by solving eq. (4.7). The Fourier–Laplace transform of $\hat{\sigma}(\boldsymbol{r},\boldsymbol{s},t)$ is defined to be

$$\sigma(\boldsymbol{k},\boldsymbol{s},\epsilon)=N^{-1/2}\sum_{\boldsymbol{r}}\int_0^\infty\mathrm{d}t\exp(-\epsilon t+\mathrm{i}\boldsymbol{k}\cdot\boldsymbol{r})\hat{\sigma}(\boldsymbol{r},\boldsymbol{s},t)\,, \tag{4.8}$$

and the Liouville space Green function G is given by

$$\sigma(\boldsymbol{k},\boldsymbol{s},\epsilon)=\sum_{\boldsymbol{s}'}G_{\boldsymbol{s}\boldsymbol{s}'}(\boldsymbol{k},\epsilon)\Big(N^{-1/2}\sum_{\boldsymbol{r}}\exp(\mathrm{i}\boldsymbol{k}\cdot\boldsymbol{r})\hat{\sigma}(\boldsymbol{r},\boldsymbol{s}',0)\Big)\,, \tag{4.9}$$

We have developed a novel procedure based on the Liouville space t-matrix, by which $G_{\boldsymbol{s}\boldsymbol{s}'}(\boldsymbol{k},\epsilon)$ can be obtained in closed form. This method is described in appendix A of ref. [10]. The final result is

$$G_{\boldsymbol{s}\boldsymbol{s}'}(\boldsymbol{k},\epsilon)=G^{(0)}_{\boldsymbol{s}\boldsymbol{s}'}(k,\epsilon)+G^{(0)}_{0\boldsymbol{s}'}(\boldsymbol{k},\epsilon)K_{\boldsymbol{s}}(\boldsymbol{k},\epsilon)/[1-\Gamma(\epsilon)K_{\boldsymbol{0}}(\boldsymbol{k},\epsilon)]\,, \tag{4.10a}$$

where

$$K_{\boldsymbol{s}}(k,\epsilon)=\sum_{\boldsymbol{s}'}f(\boldsymbol{s}')G_{\boldsymbol{s}\boldsymbol{s}'}(\boldsymbol{k},\epsilon)\,, \tag{4.10b}$$

and

$$G^{(0)}_{\boldsymbol{s}\boldsymbol{s}'}(\boldsymbol{k},\epsilon)=N^{-1}\sum_{\boldsymbol{q}}\exp[\mathrm{i}\boldsymbol{q}\cdot(\boldsymbol{s}-\boldsymbol{s}')]\Big(\epsilon+\Gamma(\epsilon)+2\sum_{\boldsymbol{a}}\exp(\mathrm{i}\boldsymbol{q}\cdot\boldsymbol{a})\langle J(\boldsymbol{a})\rangle\sin(\boldsymbol{k}\cdot\boldsymbol{a}/2)\Big)^{-1}\,. \tag{4.10c}$$

$\Gamma(\epsilon)$ is the Laplace transform of $\hat{\Gamma}(t)$,

$$\Gamma(\epsilon)=\int_0^\infty\mathrm{d}t\exp(-\epsilon t)\,\hat{\Gamma}(t)\,. \tag{4.11}$$

In sections 6 and 7, we shall make the following choice for $f(\boldsymbol{s})$,

$$f(\boldsymbol{s})=\delta_{\boldsymbol{s},0}\,. \tag{4.12}$$

For this choice of $f(s)$, eqs. (4.10a)–(4.10c) assume the form

$$G_{ss'}(k,\epsilon)=G^{(0)}_{ss'}(k,\epsilon)+G^{(0)}_{s0}(k,\epsilon)G^{(0)}_{0s'}(k,\epsilon)\Gamma(\epsilon)/[1-\Gamma(\epsilon)Q(k,\epsilon)]\,, \tag{4.13a}$$

with

$$Q(k,\epsilon)\equiv G^{(0)}_{00}(k,\epsilon)\,. \tag{4.13b}$$

The transport properties of the quantum particle can be determined from $\mathscr{P}(r,t)$, the probability that the particle undergoes a displacement r in time t. $P(k,\epsilon)$, the Fourier–Laplace transform (eq. (4.8)) of $\mathscr{P}(r,t)$ is related to the Green function by

$$P(k,\epsilon)=G_{00}(k,\epsilon)\,. \tag{4.14}$$

The generalized wavevector and frequency-dependent diffusion coefficient $D(k,\epsilon)$ is defined by

$$P(k,\epsilon)\equiv[\epsilon+k^2D(k,\epsilon)]^{-1}\,, \tag{4.15}$$

and is related to $\Gamma(\epsilon)$ by

$$k^2D(k,\epsilon)=Q^{-1}(k,\epsilon)-\Gamma(\epsilon)-\epsilon\,. \tag{4.16}$$

If $D(k,\epsilon)$ approaches a finite value $D(0,0)$ for small ϵ and k, then in this limit, $P(k,\epsilon)$ assumes the form of the propagator of a diffusion equation with diffusion constant $D(0,0)$. Eq. (4.16) shows that if $\Gamma(\epsilon)$ approaches a finite limit for small frequencies, then $D(0,0)$ exists, and transport is diffusive at long times and for large displacements. Let us consider the implications of an infrared divergence of $\Gamma(\epsilon)$: $\Gamma(\epsilon)\propto\epsilon^{-\alpha}$, where $\alpha>0$. For $\Gamma(\epsilon)\gg\langle J(a)\rangle$, eq. (4.16) becomes

$$k^2D(k,\epsilon)=\frac{4}{\epsilon+\Gamma(\epsilon)}\sum_a\langle J(a)\rangle^2\sin^2(k\cdot a/2)\,. \tag{4.17}$$

For an isotropic lattice in which the small wavevector limit of $D(k,\epsilon)$ is independent of the direction of k, then the $k\to0$ limit of eq. (4.17) in d dimensions is

$$D(0,\epsilon)=\frac{1}{d[\epsilon+\Gamma(\epsilon)]}\sum_a a^2\langle J(a)\rangle^2\,. \tag{4.18}$$

Eq. (4.18) shows that if $\Gamma(\epsilon)$ has an infrared divergence, $\Gamma(\epsilon)\propto\epsilon^{-\alpha}$, then $D(0,\epsilon)$ vanishes as ϵ^{α}. The mean-squared displacement of the particle $\langle r^2(t)\rangle$ is related to the diffusion coefficient by

$$\int_0^\infty \mathrm{d}t\exp(-\epsilon t)\,\langle r^2(t)\rangle=2d\epsilon^{-2}D(0,\epsilon)\,. \tag{4.19}$$

Application of the Tauberian theorem for Laplace transforms [19] shows that if $D(0,\epsilon)$ vanishes as ϵ^{α}, then $\langle r^2(t)\rangle$ is proportional to $t^{1-\alpha}$. If $\alpha=1$, then $\langle r^2(t)\rangle$ reaches a finite limit at long times, and the particle is localized. For $0<\alpha<1$, $\langle r^2(t)\rangle$ is unbounded but increases more slowly than in the diffusive case ($\alpha=0$). The case in which $0<\alpha<1$ is known as weak localization [20].

The reduced equation of motion introduced in this section (eq. (4.7)) can be used to describe the motion of particles (rather than excitations) in a disordered medium. In that case, we shall introduce the complex electrical conductivity $\sigma(\omega)$ which is related to the diffusion coefficient by [9]

$$\sigma(\omega)=(ne^2/kT)D(0,\mathrm{i}\omega)\,, \tag{4.20a}$$

where

$$\sigma(\omega)=\sigma'(\omega)+\mathrm{i}\sigma''(\omega)\,. \tag{4.20b}$$

$\sigma'(\omega)$ and $\sigma''(\omega)$ are the real and imaginary parts of the complex conductivity, respectively, n is the number density of charge carriers, and e is the magnitude of their electrical charge. The ac conductivity is proportional to $\sigma'(\omega)$. If $\alpha=1$, then $\sigma'(\omega)\propto\omega$ for small frequencies, and the system has zero dc conductivity. If $\alpha=0$, the dc conductivity is finite. Thus, the existence of a metal–insulator phase transition implies critical behavior for $\Gamma(\epsilon)$. The effective dephasing approximation (EDA) which will be presented in sections 6 and 7 is based on mapping specific models of disorder into eq. (4.7) and determining $\Gamma(\epsilon)$ self-consistently.

5. The effective dephasing rate as a generalized strong collision operator

We can gain further insight into the physical significance of the reduced equation of motion (eq. (4.7)) and of $\hat{\Gamma}(t)$ and $f(\boldsymbol{s})$ by transforming to the Wigner representation [11,21,22]. The Wigner phase space distribution function $\phi(\boldsymbol{r},\boldsymbol{p},t)$ is defined by

$$\phi(\boldsymbol{r},\boldsymbol{p},t)=N^{-1}\sum_{\boldsymbol{s}}\exp(\mathrm{i}\boldsymbol{p}\cdot\boldsymbol{s}/\hbar)\hat{\sigma}(\boldsymbol{r},\boldsymbol{s},t)\,. \tag{5.1}$$

N is the number of lattice sites. Eq. (5.1) is the discretized version of the usual Wigner function, in which $\boldsymbol{r}$ and $\boldsymbol{p}$ are continuous variables. Applying the Wigner transform in eq. (5.1) to eq. (4.7) yields the equation of motion of $\phi(\boldsymbol{r},\boldsymbol{p},t)$

$$\dot{\phi}(\boldsymbol{r},\boldsymbol{p},t)=2\sum_{\boldsymbol{a}}\langle J(\boldsymbol{a})\rangle\sin(\boldsymbol{p}\cdot\boldsymbol{a}/\hbar)\phi(\boldsymbol{r}+\boldsymbol{a}/2,\boldsymbol{p},t)$$

$$+\int_0^t \mathrm{d}\tau\,\hat{\Gamma}(t-\tau)\sum_{\boldsymbol{p}'}[F(\boldsymbol{p})\phi(\boldsymbol{r},\boldsymbol{p}',\tau)-F(\boldsymbol{p}')\phi(\boldsymbol{r},\boldsymbol{p},\tau)]\,, \tag{5.2a}$$

$$F(\boldsymbol{p})=N^{-1}\sum_{\boldsymbol{s}}\exp(\mathrm{i}\boldsymbol{p}\cdot\boldsymbol{s}/\hbar)f(\boldsymbol{s})\,. \tag{5.2b}$$

$F(\boldsymbol{p})$, the Wigner transform of $f(\boldsymbol{s})$, is normalized according to

$$f(0)=\sum_{\boldsymbol{p}}F(\boldsymbol{p})=1\,. \tag{5.2c}$$

The first term on the rhs of eq. (5.2a) represents the free (coherent) motion of the particle on an ordered lattice. If we take $\hat{\Gamma}(t)=\gamma\delta(t)$, then the second term has the form of the BGK strong-collision operator in the Boltzmann equation, in which γ is the collision rate and $F(\boldsymbol{p})$ is the distribution of momentum after a collision [23]. The choice of $f(\boldsymbol{s})$ taken in eq. (4.12) corresponds to the equilibrium momentum distribution:

$$\begin{aligned}F(\boldsymbol{p})&=1/N\,,\quad \text{if } \boldsymbol{p} \text{ is in the first Brillouin zone}\,,\\ &=0\,,\quad \text{otherwise}\,.\end{aligned} \tag{5.3}$$

According to eq. (5.3), the momentum is uniformly distributed after each collision. This choice will be adopted in the following sections. The transformation to the Wigner representation shows that the generalized dephasing rate $\hat{\Gamma}(t)$ can be regarded as a generalized collision rate in the Boltzmann equation. Eq. (5.2a) has the form of a discretized Boltzmann equation. If the transfer matrix element $\langle J(\boldsymbol{a})\rangle$ is taken to have the value J for nearest-neighbor sites and to vanish otherwise, then in the continuum limit, $\boldsymbol{p}\cdot\boldsymbol{a}/\hbar\to 0$, eq. (5.2a) becomes

$$\dot{\phi}(\boldsymbol{r},\boldsymbol{p},t)=(\boldsymbol{p}/m)\cdot\nabla\phi(\boldsymbol{r},\boldsymbol{p},t)+\int_0^t \mathrm{d}\tau\,\hat{\Gamma}(t-\tau)\int \mathrm{d}\boldsymbol{p}'\,[\tilde{F}(\boldsymbol{p})\phi(\boldsymbol{r},\boldsymbol{p}',\tau)-\tilde{F}(\boldsymbol{p}')\phi(\boldsymbol{r},\boldsymbol{p},\tau)]\,, \tag{5.4a}$$

$$m=\hbar/2Ja^2 . \tag{5.4b}$$

In eq. (5.4b), a is the lattice spacing. $\tilde{F}(p)$ is defined in analogy to $F(p)$, but has continuum normalization:

$$\int \tilde{F}(p)\,\mathrm{d}p=1 . \tag{5.5}$$

Eq. (5.4a) has the form of the Boltzmann equation in the BGK approximation of a classical particle of mass m with a generalized collision rate $\tilde{\Gamma}(t)$ [23]. We shall now sum eq. (5.2a) over the coordinate r and retain only the momentum. The result is

$$\Psi(p,t)=\int_0^t \mathrm{d}\tau\,\hat{\Gamma}(t-\tau)\,[F(p)-\Psi(p,\tau)] , \tag{5.6}$$

$$\Psi(p,t)\equiv\sum_r \phi(r,p,t) . \tag{5.7}$$

The solution of eq. (5.6), with the initial distribution $\Psi(p,0)$, is given by

$$\Psi(p,t)=\Psi(p,0)\hat{S}(t)+F(p)\,[1-\hat{S}(t)] , \tag{5.8}$$

where $\hat{S}(t)$ is the inverse Laplace transform of $S(\epsilon)$,

$$S(\epsilon)=[\epsilon+\Gamma(\epsilon)]^{-1} . \tag{5.9}$$

The bimodal distribution (eq. (5.8)) is a characteristic of strong collision models. Note that if $\Gamma(\epsilon)$ is independent of ϵ, we have

$$\hat{S}(t)=\exp(-\Gamma t) . \tag{5.10}$$

6. The effective dephasing approximation (EDA) for the Anderson model

In this section, we outline an approach by which the frequency-dependent dephasing rate $\Gamma(\epsilon)$ is determined self-consistently for the Anderson model of the motion of a particle on a lattice with diagonal disorder. We consider a quantum particle or excitation, whose motion is described by the tight-binding Hamiltonian in eq. (4.1). The site energies $\{E_x\}$ are assumed to be independent random variables with a distribution $R(E_x)$, and the transfer matrix elements $J(x-x')$ are taken to have the value J for nearest-neighbor sites, and to vanish otherwise. The EDA self-consistent equation for $\Gamma(\epsilon)$ is derived by considering two dynamical quantities: $\Gamma(\epsilon)$ and $P_0(\epsilon)$, the Laplace transform of $\mathscr{P}_0(t)$. $\mathscr{P}_0(t)$ is the averaged probability that the particle is located at the same position at time t that it occupied at time zero. Inversion of the Fourier transform in eq. (4.15) at $r=0$ yields

$$P_0(\epsilon)=\Omega^{-1}\int \mathrm{d}k\,[\epsilon+k^2D(k,\epsilon)]^{-1} . \tag{6.1}$$

The integration in eq. (6.1) is carried out over the first Brillouin zone, whose "volume" is Ω. Eq. (6.1) is an exact relation between $P_0(\epsilon)$ and $D(k,\epsilon)$. $D(k,\epsilon)$ is related to $\Gamma(\epsilon)$ in eq. (4.16). Eq. (6.1) thus provides one relation between $\Gamma(\epsilon)$ and $P_0(\epsilon)$. We require a second relation between these quantities in order to have a closed equation. In ref. [10], a second, approximate relation between these two quantities is derived. This relation is based on a comparison of the short time (large ϵ) expansions of the approximate propagator $P(k,\epsilon)$ in eq. (4.14) and of the exact propagator for the Anderson model,

$$\Gamma(\epsilon)=\Gamma_0+2\bar{J}^2P_0(\epsilon) , \tag{6.2a}$$

$$\hbar^2\bar{\Delta}^2=\int_{-\infty}^{\infty} dE\, E^2 R(E)\,. \tag{6.2b}$$

In eq. (6.2b), $\hbar^2\bar{\Delta}^2$ is the second moment of the distribution of site energies. Eq. (6.2a) contains a frequency-independent dephasing rate Γ_0, that accounts for processes not included in the Hamiltonian of eq. (4.1), such as electron–phonon scattering. In the Anderson model we have $\Gamma_0=0$. The role of Γ_0 will be discussed later in this section. Substitution of eq. (6.2a) into eq. (6.1), and making use of the relation between $D(\boldsymbol{k}, \epsilon)$ and $\Gamma(\epsilon)$ in eq. (4.16) yields a closed equation for the dephasing rate, that we shall denote the EDA equation:

$$\Gamma(\epsilon)=\Gamma_0+2\bar{\Delta}^2\Omega^{-1}\int d\boldsymbol{k}\,[Q(\boldsymbol{k},\epsilon)^{-1}-\Gamma(\epsilon)]^{-1}\,, \tag{6.3a}$$

$$Q(\boldsymbol{k},\epsilon)=\pi^{-d}\int_0^{\pi} dq_1\ldots\int_0^{\pi} dq_d\left(\epsilon+\Gamma(\epsilon)+4iJ\sum_{j=1}^{d}\sin(q_j)\sin(k_j/2)\right)^{-1}, \tag{6.3b}$$

$$k_j=\boldsymbol{k}\cdot\boldsymbol{x}_j\,. \tag{6.3c}$$

$\boldsymbol{x}_j$ is the lattice vector in the jth direction. $Q(\boldsymbol{k}, \epsilon)$ is defined for any $J(\boldsymbol{a})$ in eq. (4.13b). d is the spatial dimensionality. The EDA self-consistent equation predicts the existence of a metal–insulator transition in three dimensions for $\Gamma(\epsilon)$, and assumes a simple form in the vicinity of the transition [10,11]. If the particle is localized, the frequency-dependent diffusion coefficient $D(0, \epsilon)$ vanishes as ϵ approaches zero, which implies an infrared divergence in $\Gamma(\epsilon)$ (eq. (4.18)). If the particle is delocalized, $D(0, 0)$ is finite, but becomes arbitrarily small in the vicinity of the critical point, which implies that $\Gamma(0)$ becomes arbitrarily large. Thus, in the vicinity of the transition, on either side of the critical point, the condition $\Gamma(\epsilon)\gg J$ is satisfied for sufficiently small ϵ. The form of the EDA equation in this limit can be derived by substituting eq. (4.17) rather than eq. (4.16) into eq. (6.1). The result is

$$\Gamma(\epsilon)=\Gamma_0+\tfrac{1}{2}\chi[\epsilon+\Gamma(\epsilon)]I_d(\epsilon[\epsilon+\Gamma(\epsilon)]/4J^2)\,, \tag{6.4a}$$

where

$$\chi\equiv\bar{\Delta}^2/J^2\,. \tag{6.4b}$$

$I_d(y)$, the diagonal element of the Green function of the d-dimensional analog of a simple cubic lattice, is given by

$$I_d(y)=\pi^{-d}\int_0^{\pi} dk_1\ldots\int_0^{\pi} dk_d\left(y+d-\sum_{j=1}^{d}\cos(k_j)\right)^{-1}. \tag{6.5}$$

The argument of I_d in eq. (6.4a) becomes arbitrarily small in the vicinity of the critical point, so that the behavior of the solution of eq. (6.4a) near the transition can be determined from the limiting behavior of $I_d(y)$ for small y [10,24–26]

$$\begin{aligned}\lim_{y\to 0} I_d(y)&=(2y)^{-1/2}\,, && d=1\,,\\ &=-(2\pi)^{-1}\ln(y)\,, && d=2\,,\\ &=I_3(0)-\pi^{-1}(y/2)^{1/2}\,, && d=3\,.\end{aligned} \tag{6.6a}$$

$$I_3(0)\approx 0.5055\,. \tag{6.6b}$$

Substitution of eqs. (6.6a) into eq. (6.4a), and solution of the resulting equation in one and two dimensions yields the following behavior for $\Gamma(\epsilon)$. At $\chi=0$, $\Gamma(\epsilon)=\Gamma_0$. For $\chi>0$, $\Gamma(\epsilon)$ diverges as ϵ^{-1} for small frequency.

The implications of these results for the motion of the particle can be obtained from eqs. (4.18) and (4.19). The particle is predicted to be localized in one and two dimensions for any finite disorder, in agreement with the scaling theory of localization [27,28]. Our criterion for localization is the limiting behavior at long times of $\langle r^2(t)\rangle$, the mean-squared displacement. If $\langle r^2(t)\rangle$ is bounded for all times, the particle is considered to be localized, and if $\langle r^2(t)\rangle$ increases linearly in time, the particle is considered to be delocalized. If $\langle r^2(t)\rangle$ increases less strongly than linearly in time, the particle is weakly localized [20]. If the particle is localized, the dc conductivity is zero, and if the particle is delocalized, the dc conductivity is finite (eq. (4.20a)). Substitution of eq. (6.6a) with $d=3$ into eq. (6.4a) yields a self-consistent equation for $\Gamma(\epsilon)$, which is cubic in $\Gamma^{1/2}$, that is valid in the vicinity of the critical point in three dimensions.

$$[\Gamma(\epsilon)/\Gamma_0]\{1-\chi/\chi^*+(\chi/2\pi)[\epsilon\Gamma(\epsilon)/8J^2]^{1/2}\}=1\,. \tag{6.7a}$$

Eq. (6.7a) predicts a metal–insulator transition at $\chi=\chi^*$, where χ^* is given by

$$\chi^*=2/I_3(0)\approx 3.957\,. \tag{6.7b}$$

For $\chi>\chi^*$, $\Gamma(\epsilon)$ diverges as ϵ^{-1} as $\epsilon\to 0$. For $\chi<\chi^*$, $\Gamma(\epsilon)$ approaches a finite limit as $\epsilon\to 0$. At $\chi=\chi^*$, $\Gamma(\epsilon)$ diverges as $\epsilon^{-1/3}$. χ^* has been estimated by a variety of numerical methods for the original Anderson model, in which the site energies are uniformly distributed between $-W/2$ and $W/2$. The extent of the disorder is characterized by W/J, which is related to χ by

$$W/J\equiv\sqrt{12\chi}\,. \tag{6.8}$$

Recent results for the critical value of W/J are 14.9 ± 0.4 [29], 14.5 [30], 19.0 ± 0.5 [31], 16.5 ± 0.5 [32], and 15.95 ± 0.25 [33]. Our value of $\chi^*\approx 3.957$ corresponds to $(W/J)^*\approx 6.9$. The analytical EDA approach yields a prediction for $(W/J)^*$ that is within a factor of two of the current numerical predictions. Solving eq. (6.7) for $\Gamma(\epsilon)$ allows us to calculate $D(0,\epsilon)$ from eq. (4.18), $\langle r^2(t)\rangle$ from eq. (4.19), and $\mathscr{P}_0(t)$ from the inverse Laplace transform of eq. (6.2a). We then get

$$\begin{aligned} D(0,\epsilon)&=(2J^2a^2/\Gamma_0)(1-\chi/\chi^*)\,, && \chi<\chi^*\,,\\ &=a^2[(4\pi/\chi)(\chi/\chi^*-1)]^{-2}\epsilon && \chi>\chi^*\,,\\ &=a^2(J^2\chi^*/2^{3/2}\pi\Gamma_0)^{2/3}\epsilon^{1/3}\,, && \chi=\chi^*\,; \end{aligned} \tag{6.9}$$

$$\begin{aligned} \Gamma(\epsilon)&=\Gamma_0(1-\chi/\chi^*)^{-1}-\epsilon^{1/2}(\chi/2\pi)\Gamma_0^{3/2}(8J^2)^{-1/2}(1-\chi/\chi^*)^{-5/2}\,, && \chi<\chi^*\,,\\ &=8J^2[(2\pi/\chi)(\chi/\chi^*-1)]^2\epsilon^{-1}+2\Gamma_0(\chi/\chi^*-1)^{-1}\,, && \chi>\chi^*\,,\\ &=(4\sqrt{2}\pi\Gamma_0 J/\chi^*)^{2/3}\epsilon^{-1/3}\,, && \chi=\chi^*\,; \end{aligned} \tag{6.10}$$

$$\begin{aligned} \mathscr{P}_0(t)&=t^{-3/2}(2\bar{J}^2)^{-1}(\chi/2\pi)\Gamma_0^{3/2}(8J^2)^{-1/2}(1-\chi/\chi^*)^{-5/2}\,, && \chi<\chi^*\,,\\ &=4(J/\bar{J})^2[(2\pi/\chi)(\chi/\chi^*-1)]^2\,, && \chi>\chi^*\,,\\ &=t^{-2/3}(2\bar{J}^2)^{-1}(2^{5/2}\pi\Gamma_0 J/\chi^*)^{2/3}\,, && \chi=\chi^*\,; \end{aligned} \tag{6.11}$$

$$\begin{aligned} \langle r^2(t)\rangle&=2tJ^2a^2(1-\chi/\chi^*)/\Gamma_0\,, && \chi<\chi^*\,,\\ &=a^2[(4\pi/\chi)(\chi/\chi^*-1)]^{-2}\,, && \chi>\chi^*\,,\\ &=t^{2/3}a^2(J^2\chi^*/2^{3/2}\pi\Gamma_0)^{2/3}\,, && \chi=\chi^*\,. \end{aligned} \tag{6.12}$$

In eqs. (6.9) and (6.12), a is the lattice spacing. In the delocalized regime ($\chi<\chi^*$), the transport is diffusive at long times: $\langle r^2(t)\rangle$ increases linearly with time, and $\mathscr{P}_0(t)$ decays as $t^{-3/2}$. In the localized regime ($\chi>\chi^*$), $\langle r^2(t)\rangle$ is bounded, and $\mathscr{P}_0(t)$ decays to a nonzero value, indicating that there is a finite probability at all times that the particle is to be found at its original site. At the critical point ($\chi=\chi^*$), the particle is weakly localized.

$\langle r^2(t)\rangle$ increases as $t^{2/3}$, and $\mathscr{P}_0(t)$ decays at $t^{-2/3}$. For $\chi>\chi^*$, $D(0,\epsilon)$ is linear in ϵ for small ϵ, with a coefficient that diverges as $(\chi-\chi^*)^{-2\nu}$. For $\chi<\chi^*$, $D(0,\epsilon)$ approaches a constant value at small ϵ that vanishes as $(\chi^*-\chi)^s$. The critical exponents in eq. (6.9) are $\nu=1$ and $s=1$, which obey the scaling relation of Wegner, $s=(d-2)\nu$ [28]. Numerical estimates of the exponent ν range from 0.6 to 1.8 [31–34]. As discussed in refs. [8–11], the critical exponents in eqs. (6.9)–(6.12) are identical to those obtained by Vollhardt and Wölfle [35] for a gas of noninteracting fermions at zero temperature in a random potential. A comparison between their self-consistent equation for the diffusion kernel, which was derived with a diagrammatic approach, and eq. (6.4a) is made in ref. [8]. The limiting behavior of the complex conductivity at small frequencies near the transition can be determined from eqs. (4.20):

$$\sigma'(\omega)=\sigma_0(1-\chi/\chi^*)+A_1(1-\chi/\chi^*)^{-1/2}\omega^{1/2}, \quad \chi<\chi^*,$$

$$\sigma''(\omega)=A_1(1-\chi/\chi^*)^{-1/2}\omega^{1/2}, \quad \chi<\chi^*,$$

$$\sigma'(\omega)=A_2(\chi/\chi^*-1)^{-5}\omega^2, \quad \chi>\chi^*,$$

$$\sigma''(\omega)=A_3(\chi/\chi^*-1)^{-2}\omega, \quad \chi>\chi^*,$$

$$\sigma'(\omega)=A_4\omega^{1/3}, \quad \chi=\chi^*,$$

$$\sigma''(\omega)=\sigma'(\omega)/\sqrt{3}, \quad \chi=\chi^*; \tag{6.13a}$$

$$\sigma_0=(ne^2/kT)2J^2a^2/\Gamma_0,$$

$$A_1=\sigma_0\chi\Gamma_0^{1/2}/8\pi J, \quad A_2=\sigma_0\chi^4\Gamma_0^2/2^9\pi^4J^4, \quad A_3=\sigma_0\chi^2\Gamma_0/32\pi^2J^2, \quad A_4=\sigma_0\Gamma_0^{1/3}(\chi^*/\pi J)^{2/3}\sqrt{3}/8. \tag{6.13b}$$

The ac conductivity is proportional to $\sigma'(\omega)$. The dc conductivity is zero for $\chi\geq\chi^*$, and is finite for $\chi<\chi^*$. The critical behavior of transport properties within the EDA can thus be determined analytically.

This concludes our discussion of the asymptotic (long time and small frequency) behavior of the Anderson model in the vicinity of the transition. Before turning to a more general analysis of the model, valid for any time scale, we should comment on the role of the external dephasing Γ_0 and its interplay with the localization, as shown in eqs. (6.9)–(6.13). This will allow a direct comparison of the present results with the original Anderson model which assumes $\Gamma_0=0$. If we approach the transition from above ($\chi>\chi^*$), i.e., from the localized side, we note that the existence of the transition, the critical disorder, and the critical behavior are independent of Γ_0. When the transition is approached from the delocalized side ($\chi<\chi^*$), Γ_0 makes the motion incoherent (diffusive) with a diffusion constant $D\approx J^2a^2/\Gamma_0$. The reason why Γ_0 is irrelevant in the vincinity of the transition from above, is that for $\chi>\chi^*$, $\Gamma(\epsilon)$ diverges as ϵ^{-1} and is dominating the dephasing. The inclusion of Γ_0 in our model restricts our asymptotic analysis to time scales $t\ll\Gamma_0^{-1}$. Since Γ_0 can be made arbitrarily small, Γ_0^{-1} may correspond to arbitrary long time scales, so that our analysis holds for any physically realistic time scale. In conclusion, it should be emphasized that had we been interested in approaching the transition only from the localized end (as is done in other self-consistent procedures) [5], we could have simply set $\Gamma_0=0$ without affecting our analysis. The inclusion of Γ_0 allows us to approach the transition also from the conducting (delocalized) end. In that case, Γ_0 makes the electron motion incoherent.

We next turn to the calculation of transport properties for any time scale and degree of disorder, using eqs. (6.3). Evaluation of the right side of eq. (6.3a) involves performing $2d$ nested integrations over $\{q_j\}$ and $\{k_j\}$. We shall make a simplifying approximation [11] to reduce the number of integrations. In evaluating the right side of eq. (6.3b), we shall make the replacement

$$\sum_{j=1}^{d}\sin(q_j)\sin(k_j/2)\rightarrow\sin(q_1)\sin(k_1/2). \tag{6.14a}$$

The integration over q_1 can then be carried out analytically to yield

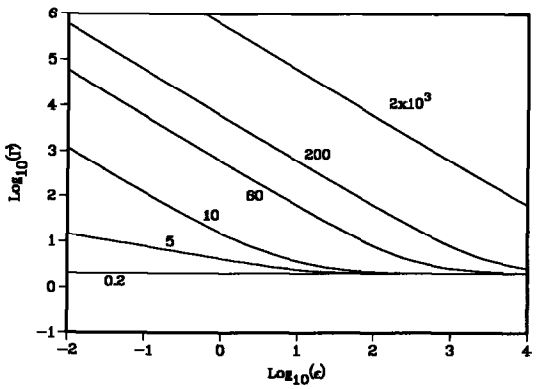

Fig. 6. The frequency-dependent dephasing rate for the Anderson model is calculated by a numerical solution of eqs. (6.3) for a simple cubic lattice [11]. The transition occurs at $(W/J)^* \approx 5.34$. Each curve is labeled by the value of W/J. $\Gamma_0 = 2J$. For $W/J > (W/J)^*$, $\Gamma(\epsilon)$ diverges as ϵ^{-1} for small ϵ, whereas for $W/J < (W/J)^*$ it approaches a constant limit.

$$Q(\boldsymbol{k}, \epsilon) = \{[\epsilon + \Gamma(\epsilon)]^2 + 16J^2 \sin^2(ka/2)\}^{-1/2} . \tag{6.14b}$$

Since $Q(\boldsymbol{k}, \epsilon)$ in eq. (6.14b) depends only on the magnitude of $\boldsymbol{k}$, of the integration over $\boldsymbol{k}$ in eq. (6.3a) reduces to a one-dimensional integral:

$$\Gamma(\epsilon) = \Gamma_0 + 2d\bar{A}^2 (a/\pi)^d \int k^{d-1}\, dk [Q(k, \epsilon)^{-1} - \Gamma(\epsilon)]^{-1} . \tag{6.15}$$

As discussed in ref. [11], the critical exponents predicted by eq. (6.15) are identical with those predicted by eqs. (6.3), although the value of χ^* is slightly different. In fig. 6, we display $\Gamma(\epsilon)$ for various values of W/J, as indicated. For $W/J > (W/J)^*$, $\Gamma(\epsilon)$ diverges as ϵ^{-1}, as $\epsilon \to 0$, whereas for $W/J < (W/J)^*$, it approaches a finite value in this limit. In fig. 7a, we display the ac conductivity $\sigma'(\omega)$ for various values of $W/J - (W/J)^*$ as indicated. The same calculations are displayed on a log–log scale in fig. 7b. The frequency dependence obtained in our analytical analysis (eqs. (6.13)) is clearly demonstrated. In fig. 8, we display the dc conductivity versus $W/J - (W/J)^*$. The dc conductivity vanishes linearly as $[(W/J)^* - (W/J)]$ for $W/J < (W/J)^*$, as predicted by eqs. (6.13).

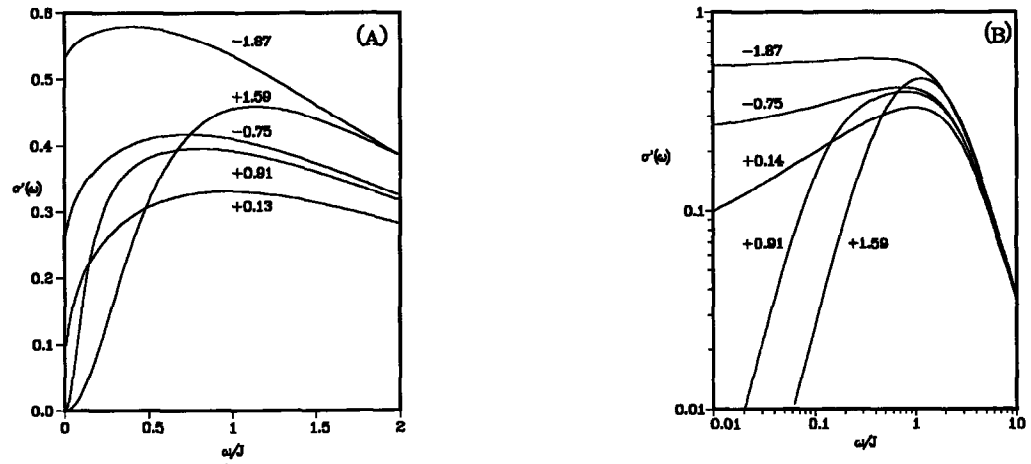

Fig. 7. (a) The ac conductivity for the Anderson model $\sigma'(\omega)$ is calculated for a simple cubic lattice [11]. $\sigma_0 = 1$. Each curve is labeled by the value of $W/J - (W/J)^*$. $\Gamma_0 = 2J$. (b) The calculations of (a) are presented in a log–log graph to illustrate the power law frequency dependence of the ac conductivity in different frequency regimes. For $W/J < (W/J)^*$, $\sigma'(\omega)$ approaches a finite limit as $\omega \to 0$: the dc conductivity. For $W/J > (W/J)^*$, $\sigma'(\omega)$ vanishes as ω^2 for small ω. For $\omega/J \gg 1$, $\sigma'(\omega)$ decays as ω^{-2} for all W/J.

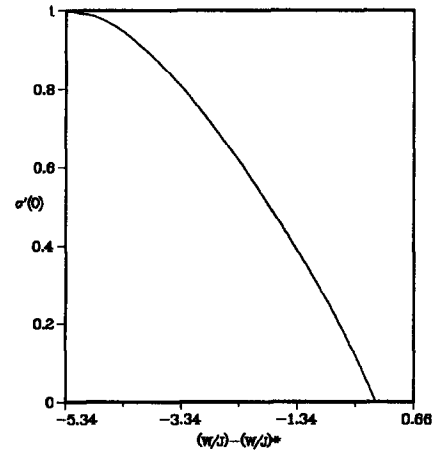

Fig. 8. The dc conductivity for the Anderson model [11] $\sigma'(0)$ is shown as a function of $W/J-(W/J)^*.\sigma_0=1$. The calculation was made using eqs. (6.3). For $W/J<(W/J)^*$ the motion of the carrier is diffusive at long times, and $\sigma'(0)$ is finite. As W/J approaches $(W/J)^*\approx 5.34$, $\sigma'(0)$ vanishes linearly with $W/J-(W/J)^*$. For $W/J>(W/J)^*$, the carrier is localized, and $\sigma'(0)$ is zero.

7. Carrier motion in dynamically disordered systems

The interaction of an electronic excitation or a charge carrier with the nuclear degrees of freedom of the surrounding medium is a central topic in the chemistry and physics of condensed phases. Such interactions play a crucial role in the dynamics of excess electrons in solids (the polaron problem) [7], in solution [36–38] and in the electrical conductivity of disordered materials such as solid electrolytes [39,40]. The problem of carrier motion in a condensed phase medium is considerably simplified, when the correlation time of the medium is short compared to the time scale of the carrier dynamics. In this case, it is possible to construct an effective Liouville operator for the carrier, in which the effect of the medium is given by a dephasing rate or friction. The Haken–Strobl model [18] of exciton motion in molecular crystals, in which the phonons enter through a dephasing rate, is based on such a separation of time scales. The reduced equation of motion for the Haken–Strobl model is eq. (4.7) with $\hat{\Gamma}(t)=\gamma\delta(t)$ and $f(s)=\delta_{s,0}$. The exact solution of this equation is given in eq. (4.13a) with $\Gamma(\epsilon)=\gamma$. Alternatively, in the Wigner representation the Haken–Strobl equation of motion is eq. (5.2a) with $\hat{\Gamma}(t)=\gamma\delta(t)$ and $F(\boldsymbol{p})$ as in eq. (5.3). The Anderson model corresponds to the other extreme in which the bath motions are infinitely slow. The Anderson model is not exactly solvable, and in section 6 we developed an approximation scheme, the EDA, to calculate the transport properties. The dynamics of electronic excitations interacting with nuclear degrees of freedom whose time scale is not necessarily short or long compared to the time scale of the excitation have received considerable attention from theorists [41–48]. Sumi [41] has investigated a model of exciton dynamics in molecular crystals, in which the system is represented by an ordered lattice with site energies that are Gaussian, stochastic variables, whose fluctuations are characterized by a finite time scale (eq. (2.3)). He calculated the absorption line shape and the density of states within the coherent potential approximation (CPA). Blumen and Silbey [42] have obtained similar results for the absorption line shape for this model, using a truncated cumulant expansion. It should be emphasized that the absorption line shape and the density of states do not contain sufficient information to yield transport properties, such as the mean-squared displacement of an excitation. In general, the approximate methods that are used to calculate a line shape or density of states cannot be extended in a simple way to the calculation of transport properties, and new methods must be developed. An example is the two-particle CPA of Velicky [49–51], which, however, does not have the capacity to predict a quantum localization transition.

In this section, we extend the EDA and apply it to carrier dynamics in a condensed phase system that is characterized both by static and dynamic sources of disorder [9]. We consider a model in which noninteracting carriers move among active sites that are randomly distributed on a lattice, with site energies that are stochastic variables whose fluctuations are characterized by a time scale of arbitrary magnitude. The model treated here

unifies a variety of models that have been extensively studied in condensed matter physics. The model is characterized by three parameters: c, the concentration of active sites, Δ, the root-mean-squared magnitude of the site energy fluctations, and Λ, the inverse correlation time of the fluctuations. We consider six limiting cases: (1) For $c=1$ (ordered lattice), $\Delta>0$, and $\Lambda>0$, we recover the model of excitons in molecular crystals that was treated by Sumi [41], and by Blumen and Silbey [42]. (2) For $c=1$ and $\Delta=0$ (no energetic disorder), the model describes a perfect lattice of interacting, quantum mechanical, two-level systems [24]. (3) For $c=1$ and $\Lambda=0$ (static energy disorder), the model reduces to the Anderson model [4–6, 29–34]. (4) For $\Delta=0$ and $c<1$, the model reduces to the quantum percolation problem, which has been the subject of several recent studies [33,52–54]. (5) For $c=1$ and $\Lambda\gg\Delta$, there is a separation of time scales between the energy fluctuations and the carrier motion, and the Haken–Strobl model of exciton dynamics in molecular crystals is recovered [18]. (6) For $\Lambda\gg\Delta$ and $\Delta^2/\Lambda\gg J$, the Liouville equation reduces to a Pauli master equation with a site-to-site hopping rate of $J^2\Lambda/\Delta^2$. This limit describes incoherent exciton motion [55–57].

Our model system consists of a lattice in d dimensions with two types of sites: active sites on which the carriers may reside, and forbidden sites that are inaccessible to the carriers. A fraction c of the sites are active, and these are randomly distributed on the lattice. Since the carriers are assumed not to interact with each other, we consider the dynamics of a single carrier. For a given configuration of this random system, the single particle density matrix $\hat{\rho}$ obeys the Liouville equation:

$$\mathrm{d}\hat{\rho}/\mathrm{d}t=-\mathrm{i}[H,\hat{\rho}]\equiv-\mathrm{i}L\hat{\rho}\,, \tag{7.1a}$$

where

$$H=\sum_m\left[\bar{\omega}_{\mathrm{eg}}+\delta\omega_m(t)\right]|m\rangle\langle m|+\sum_{m,n}J_{mn}|m\rangle\langle n|\,. \tag{7.1b}$$

The sums in eq. (7.1b) run over the indices labelling the active sites. $|m\rangle$ denotes the state in which the carrier resides at the active site labelled m. J_{mn} is the transfer matrix element between active sites m and n, which we will take to have the value J if m and n are nearest neighbors on the lattice, and to vanish otherwise. $\hbar\delta\omega_m(t)$ is a stochastic variable that represents the fluctuating site energy of the active site labelled m. We adopt the same model for the fluctuations used in sections 2 and 3, i.e.,

$$\langle\delta\omega_m(t)\delta\omega_n(\tau)\rangle=\delta_{mn}\Delta^2\exp(-\Lambda|t-\tau|)\,. \tag{7.2}$$

The present model corresponds to a quantum mechanical treatment of the carrier, and a classical treatment of the medium degrees of freedom with which the carrier interacts. A microscopic model of exciton dynamics with exciton–phonon coupling that is linear in the phonon coordinates can be mapped into the present problem in an approximate fashion, in which case the parameter Δ^2 is linear in the temperature, for kT large compared to lattice vibration energies [41]. It should be noted that in such a stochastic treatment, the action of the carrier on the surrounding medium is neglected; that is, the "bath" affects the "system", but the "system" does not affect the "bath". In other words, polaron effects [7,47] are not included in this stochastic approach.

Neither the absorption spectrum nor the transport properties can be determined exactly for this model, and approximate methods must be applied. The optical absorption spectrum has been calculated for this model for $c=1$ by Sumi [41] who used the coherent potential approximation, and by Blumen and Silbey [42] who used a truncated cumulant expansion. Sumi's treatment was written in ordinary Hilbert space. We shall now rewrite his results using our Liouville space formulation. This establishes the connection between his treatment and our effective dephasing theory. We shall denote the ground state of the system in which all molecules are in the electronic ground state by $|0\rangle$. The density matrix element ρ_{m0} represents an *intramolecular coherence* on the mth site. The density of states and the optical lineshape can be expressed in terms of the following Green function, which represents the time evolution of the intramolecular coherence,

$$\hat{\rho}_{m0}(t)=\sum_n\hat{G}_{m0,n0}(t)\hat{\rho}_{n0}(0)\,. \tag{7.3}$$

This Green function is defined by

$$\hat{G}_{m0,n0}(t)=\theta(t)\left\langle a_m \exp_+\left(-\mathrm{i}\int_0^t L(\tau)\,\mathrm{d}\tau\right)a_n^\dagger\right\rangle , \tag{7.4}$$

where $a_m^\dagger$ and a_m are the creation and annihilation operators for an excitation at the site labeled m, and 0 is the lattice ground state. The angular brackets denote an electronic trace and average over the fluctuations. We define the Fourier–Laplace transform of the Green function by

$$G(\boldsymbol{k},\epsilon)=\frac{1}{N}\sum_{m,n}\int_0^\infty \mathrm{d}t\,\hat{G}_{m0,n0}(t)\exp[-\epsilon t-\mathrm{i}\boldsymbol{k}\cdot(\boldsymbol{r}_m-\boldsymbol{r}_n)]\equiv[\epsilon+\mathrm{i}L_{\mathrm{eff}}(\epsilon)]^{-1} . \tag{7.5}$$

L_{eff} is an effective Liouville operator. $\boldsymbol{r}_m$ is the position of the lattice site labelled m. Sumi has adopted the following ansatz for $G(\boldsymbol{k},\epsilon)$ (and L_{eff})

$$G(\boldsymbol{k},\epsilon)=[\epsilon+\Gamma_{\mathrm{s}}(\epsilon)+\mathrm{i}\tilde{J}(\boldsymbol{k})]^{-1} , \tag{7.6a}$$

with

$$\tilde{J}(\boldsymbol{k})=\sum_m J_{mn}\exp[-\mathrm{i}\boldsymbol{k}\cdot(\boldsymbol{r}_m-\boldsymbol{r}_n)] . \tag{7.6b}$$

The optical absorption spectrum is given by

$$\sigma(\omega)=-\pi^{-1}\,\mathrm{Re}\,G(\boldsymbol{k}=0,\,-\mathrm{i}(\omega-\bar{\omega}_{\mathrm{eg}}))=-\pi^{-1}\,\mathrm{Im}[\omega-\bar{\omega}_{\mathrm{eg}}-\tilde{J}(\boldsymbol{k}=0)+\mathrm{i}\Gamma_{\mathrm{s}}(-\mathrm{i}(\omega-\bar{\omega}_{\mathrm{eg}}))]^{-1} , \tag{7.7}$$

and the density of states is

$$\rho_{\mathrm{s}}(\omega)=-\pi^{-1}\,\mathrm{Re}\,G(\boldsymbol{k},\,-\mathrm{i}(\omega-\bar{\omega}_{\mathrm{eg}}))=-\pi^{-1}\mathrm{Im}\left\{\sum_{\boldsymbol{k}}[\omega-\bar{\omega}_{\mathrm{eg}}-\tilde{J}(\boldsymbol{k})+\mathrm{i}\Gamma_{\mathrm{s}}(-\mathrm{i}(\omega-\bar{\omega}_{\mathrm{eg}}))]^{-1}\right\} . \tag{7.8}$$

Sumi then developed the following self-consistent equation for $\Gamma_{\mathrm{s}}(\epsilon)$

$$\Gamma_{\mathrm{s}}(\epsilon)=\cfrac{\Delta^2}{\bar{F}(\epsilon+\Delta)^{-1}+\cfrac{2\Delta^2}{\bar{F}(\epsilon+2\Delta)^{-1}+\cfrac{3\Delta^2}{\bar{F}(\epsilon+3\Delta)^{-1}+\ldots}}} , \tag{7.9a}$$

$$\bar{F}(\epsilon)=[\bar{G}^{-1}(\epsilon)-\Gamma_{\mathrm{s}}(\epsilon)]^{-1} , \tag{7.9b}$$

$$\bar{G}(\epsilon)=\sum_{\boldsymbol{k}}G(\boldsymbol{k},\epsilon)\approx 2\{\epsilon+\Gamma_{\mathrm{s}}(\epsilon)+\{[\epsilon+\Gamma_{\mathrm{s}}(\epsilon)]^2+36J^2\}^{1/2}\}^{-1} . \tag{7.9c}$$

The last equality in eq. (7.9c) results from applying the Hubbard approximation to the lattice Green function [24]. If the intermolecular interaction $\tilde{J}$ is set equal to zero, then eq. (7.7) reduces to eq. (2.14), the absorption lineshape for a single molecule. In this limit, the expression for $\Gamma_{\mathrm{s}}(\epsilon)$ in eq. (7.9a) reduces to eq. (2.11), the single molecule dephasing rate.

We have developed a self-consistent theory for the transport properties of a particle or excitation governed by the Hamiltonian of eq. (7.1b). The approach is similar to the derivation of the EDA self-consistent equation

for the Anderson model in eqs. (6.3), except that the approximate relation that is used to close eq. (6.1) is based on an expansion in powers of the concentration of active sites, rather than the short time expansion that led to eq. (6.2a). The model investigated in this section is a generalization to an infinite lattice of the two-site model treated in section 3. Our treatment of the present model makes use of the exact solution of the dimer problem. A complete discussion of the derivation is given in ref. [9]. The result is the following pair of coupled equations for $P_0(\epsilon)$ and $D(\epsilon)$ [9]:

$$P_0(\epsilon)=[a^2/2D(\epsilon)]I_d(a^2\epsilon/2D(\epsilon))\,, \tag{7.10a}$$

$$D(\epsilon)=cD_0(P_0^{-1})/[1+2P_0D_0(P_0^{-1})a^{-2}]\,, \tag{7.10b}$$

where

$$D_0(y)=(aJ)^2[\Gamma_1(y)+\Gamma_2(y)+\Gamma_3(y)+\Gamma_4(y)-2y]/\{\Gamma_2(y)\Gamma_3(y)-[y-\Gamma_1(y)][y-\Gamma_4(y)]\}\,, \tag{7.10c}$$

$$k^2D(\boldsymbol{k},\epsilon)=2a^{-2}D(\epsilon)\Big(d-\sum_{n=1}^{d}\cos(\boldsymbol{k}\cdot\boldsymbol{a}_n)\Big)\,. \tag{7.10d}$$

$D(\epsilon)$ in eqs. (7.10a) and (7.10b) is the $\boldsymbol{k}\to 0$ limit of $D(\boldsymbol{k},\epsilon)$ in eq. (7.10d). I_d is defined in eq. (6.5). The lattice vector in the direction n is $\boldsymbol{a}_n$, and has a magnitude a. Γ_1, Γ_2, Γ_3 and Γ_4 denote, respectively, the matrix elements $\gamma_{12,12}$, $\gamma_{12,21}$, $\gamma_{21,12}$, $\gamma_{21,21}$ of the dephasing matrix for the dimer (eq. (3.4b)). Eqs. (7.10a) and (7.10b), can be solved for either $D(\epsilon)$ or for P_0. The solution for $D(\epsilon)$ can then be substituted into eq. (7.10d) to yield $D(\boldsymbol{k},\epsilon)$. In order to compare the solution of eqs. (7.10) to the work of Sumi, and to the results of the previous sections, we shall use eq. (4.17) to define a frequency-dependent dephasing rate for this model. Comparison of eqs. (4.17) and (7.10d) yields

$$\Gamma(\epsilon)=2J^2a^2/D(\epsilon)-\epsilon\,. \tag{7.11}$$

The transport properties of this model can then be interpreted in terms of an effective dephasing rate $\Gamma(\epsilon)$ obtained from eqs. (7.10) and (7.11). This dephasing rate is different from the function $\Gamma(\epsilon)$ obtained from eq. (7.9a) which determines the spectral properties of the medium. Later in this section we shall compare these two dephasing rates in detail. First, however, we shall determine the solution of eqs. (7.10). In order to solve eqs. (7.10a) and (7.10b), the matrix elements Γ_1 through Γ_4 must be evaluated. For arbitrary values of Δ and Λ, $\gamma(\epsilon)$ may be calculated numerically from the matrix continued fraction in eq. (3.4b). We can, however, analytically determine the asymptotic behavior of the solution of eqs. (7.10a) and (7.10b) at small frequencies, and hence long times. There are two cases to consider: $\Lambda>0$ (dynamic fluctuations) and $\Lambda=0$ (static site energy disorder). The small frequency (long time) behavior of the solution of eqs. (7.10a) and (7.10b) is different in each of these cases. We begin by considering this small frequency behavior in one, two and three dimensions for $\Lambda>0$, in which case "small frequency" means $\epsilon\ll\Lambda$. We expect that in the vicinity of a metal–insulator transition and for sufficiently small frequencies, $P_0^{-1}\ll\Lambda$. (We shall solve eqs. (7.10a)–(7.10d) within this assumption, and it is easily verified that the resulting solution is consistent with this condition.) Substitution of eq. (7.10a) into eq. (7.10b) yields a closed equation for $D(\epsilon)$. Eq. (7.11) can be used to transform this relation into the following closed equation for $\Gamma(\epsilon)$:

$$\Gamma(\epsilon)=\frac{2J^2a^2}{cD_0(0)}+\frac{\epsilon+\Gamma(\epsilon)}{c}I_d\Big(\frac{\epsilon[\epsilon+\Gamma(\epsilon)]}{4J^2}\Big)\,. \tag{7.12}$$

Eq. (7.12) has the same structure as eq. (6.4a), the EDA self-consistent equation for the Anderson model in the vicinity of the critical point. Eq. (6.4a) can be transformed into eq. (7.12) by making the following substitutions

$$\Gamma_0\to 2J^2a^2/cD_0(0)\,, \tag{7.13a}$$

$$\chi/2\to 1/c\,. \tag{7.13b}$$

Inspection of eq. (3.4b) shows that for $\Lambda > 0$, the matrix elements of $\gamma(\epsilon)$ are finite in the limit of zero ϵ. $D_0(0)$, which depends on Δ, Λ, and J, but not on P_0, can be expressed in terms of the matrix elements of $\gamma(0)$ by setting $y=0$ in eq. (7.10c). The solution of eq. (6.4a) is discussed in section 6, and the solution of eq. (7.12) can be obtained from it by making the substitutions in eq. (7.13). In $d=1$ and $d=2$, eq. (7.12) predicts that $\Gamma(\epsilon) \propto \epsilon^{-1}$, and hence that carriers are localized, in agreement with the scaling theory of Anderson localization [27,35]. In $d=3$, a metal–insulator transition is predicted at a critical value of the concentration of active sites: $c^* = I_3(0) \approx 0.5055$. The solution of eq. (7.12) in $d=3$ can be obtained from eq. (6.10) by making the substitutions in eq. (7.13). For $c > c^*$, $\Gamma(\epsilon)$ approaches a finite limiting value for small frequencies, and for $c < c^*$, it displays an infrared divergence. At $c=c^*$, $\Gamma(\epsilon) \propto \epsilon^{1/3}$. $\mathscr{P}_0(t)$ and $\langle r^2(t) \rangle$ can be determined from eqs. (6.11), (6.12) and (7.13). For $c < c^*$, $\langle r^2(t) \rangle$ reaches a finite value at long time, indicating that carriers are trapped in a finite volume. For $c > c^*$, the carrier moves diffusively at long times, with $\langle r^2(t) \rangle$ that increases linearly in time. At $c=c^*$, $\langle r^2(t) \rangle \propto t^{2/3}$. The carriers are not trapped, but their motion is less efficient than ordinary diffusion. This phenomenon is referred to as weak localization [59] or anomalous diffusion [60].

We have determined the long time and small frequency behavior of the transport properties calculated from eqs. (7.12) for $\Lambda > 0$ in terms of $D_0(0)$, as a function of J, Δ, and Λ. D_0 is defined in terms of the matrix elements of $\gamma(\epsilon)$ by eq. (7.10c). In general, these matrix elements must be determined numerically from the matrix continued fraction expression for $\gamma(\epsilon)$ in eq. (3.4b). However, D_0 can be determined in closed form in the limit $\Lambda \gg \Delta$. In this limit, the correlation time of the site energy fluctuations is small compared to the inverse magnitude of the fluctuations. Under these conditions, the continued fraction in eq. (3.4b) can be truncated to yield $\gamma(\epsilon) = 2(\Delta^2/\Lambda)\mathbf{B}^2$. Substituting this result into eq. (7.10c) yields $D_0(0)$ in the dynamic limit ($\Lambda \gg \Delta$):

$$D_0(0) = J^2 a^2 \Lambda / \Delta^2 . \tag{7.14}$$

In figs. 9a and 10a, we display the effective dephasing relevant for the optical spectra and density of states, obtained by numerically solving eqs. (7.9). In fig. 9a, the energy disorder is almost static $\Lambda/6J = 10^{-4}$. The various curves are for different values of $\Delta/6J$ as indicated. In fig. 10a, we have fixed the magnitude of the disorder $\Delta/6J = 1$ and the various curves correspond to different values of $\Lambda/6J$ (as indicated). For comparison, we present in figs. 9b and 10b the corresponding calculations of the effective dephasing relevant for transport, obtained by solving eqs. (7.10) numerically. These figures clearly show that the spectroscopic $\Gamma_s(\epsilon)$ (figs. 9a and 10a) is insensitive to the localization transition and $\Gamma_s(\epsilon)$ always attains a finite limiting value as $\epsilon \to 0$. The dephasing associated with transport $\Gamma(\epsilon)$ (figs. 9b and 10b), on the other hand, clearly shows the $1/\epsilon$ divergence

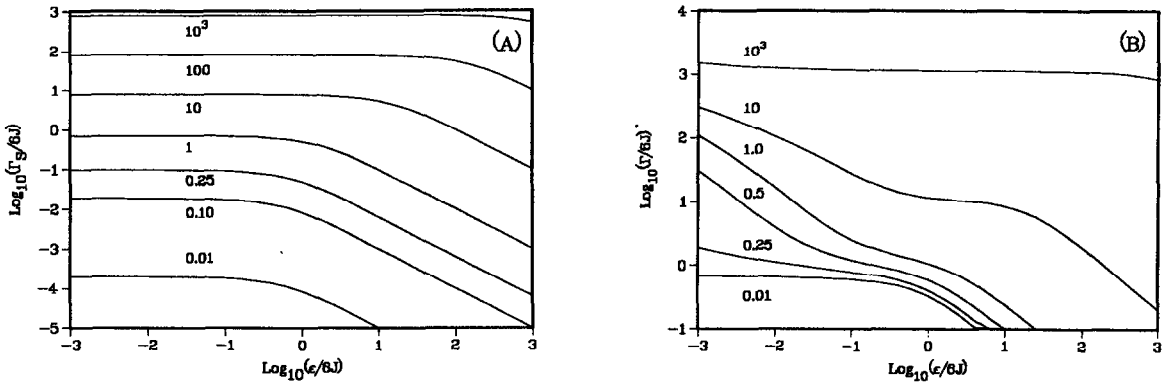

Fig. 9. (a) The frequency-dependent dephasing rate associated with the absorption lineshape is calculated using Sumi's dynamical CPA (eqs. (7.9)). $\Lambda/6J = 10^{-4}$. Each curve is labeled by the value of $\Delta/6J$. In all cases, $\Gamma_s(\epsilon)$ approaches a finite value as $\epsilon \to 0$. (b) The frequency-dependent dephasing rate associated with transport in a dynamically disordered system is calculated from eqs. (7.10) and (7.11). All other parameters are the same as in fig. 9a. Note the $1/\epsilon$ divergence of $\Gamma(\epsilon)$ near the critical point ($\Delta/6J \approx 0.37$), which is absent from fig. 9a.

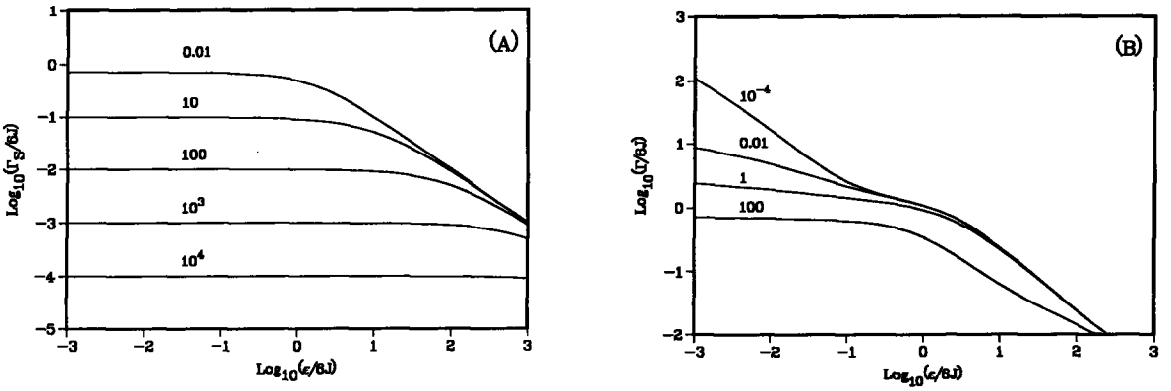

Fig. 10. (a) The frequency-dependent dephasing rate associated with the absorption lineshape is calculated using Sumi's dynamical CPA (eqs. (7.9)). $\Delta/6J=1$. Each curve is labeled by the value of $\Delta/6J$. In all cases, $\Gamma_s(\epsilon)$ attains a finite limiting value as $\epsilon\to 0$. (b) The frequency-dependent dephasing rate for transport with dynamical disorder is calculated from eqs. (7.10) and (7.11). All other parameters are the same as in (a). Note the $1/\epsilon$ divergence of $\Gamma(\epsilon)$ as $\epsilon\to 0$.

which is the signature of localization. It is interesting to note that for the Haken–Strobl model ($\Lambda\gg\Delta$), both dephasing rates are independent of frequency and the dephasing rate associated with transport $\Gamma=2\Delta^2/\Lambda$, is simply twice the spectroscopic dephasing rate $\Gamma_s=\Delta^2/\Lambda$. When the medium time scale is finite, the two dephasing rates are, however, significantly different as illustrated in figs. 9 and 10.

We next turn to the analysis of the solution of eqs. (7.10) for $\Lambda=0$. In this limit, the site energies are static, random variables with a Gaussian distribution. In the absence of topological disorder, $c=1$, this model reduces to the Anderson model of a lattice with random site energies [8,9,29–34], which was treated in section 6. For $\Lambda=0$, eqs. (7.10a)–(7.10d) do not reduce to eq. (7.12) as they did for nonzero Λ. The derivation of eq. (7.12) relies on the fact that the limit of $D_0(y)$ in eq. (7.10c) as y approaches zero is finite. This limit exists for $\Lambda>0$, but is undefined for $\Lambda=0$. In the static limit, the continued fraction expression for the dimer dephasing matrix in eq. (3.4b), whose matrix elements enter into eq. (7.10c), converges increasingly slowly as ϵ is decreased. It is thus inconvenient to analyze eqs. (7.10) directly in the limit of small ϵ at $\Lambda=0$. The $\Lambda=0$ limit of eqs. (7.10) is derived in ref. [9], and is presented in eq. (4.16) of that work. This relation is derived by determining the dimer Green function $G(\epsilon)$ in eq. (3.4a) by calculating $G(\epsilon)$ for a pair of sites with given site energies, and then averaging over a static, Gaussian distribution of site energies. The resulting expression is equivalent to the $\Lambda=0$ limit of the continued fraction in eq. (3.4b). It is found that carriers are always localized for $d=1$ and $d=2$. In $d=3$, a metal–insulator transition is found to take place at a critical concentration c^* given by

$$c^*=I_3(0)/H(J/\Delta)\,, \tag{7.15a}$$

with

$$H(y)\equiv\pi^{1/2}y\exp(y^2)\,\mathrm{erfc}(y)\,. \tag{7.15b}$$

The critical concentration is a function of the magnitude of the site energy disorder. For $\Delta\ll J$ (weak energetic disorder), $H(J/\Delta)\approx 1$, and $c^*=I_3(0)\approx 0.5055$. c^* increases as the magnitude of the energetic disorder is increased. As Δ/J is increased, c^* increases without bound, according to eq. (7.15b). Of course, c, the fraction of active sites cannot exceed unity. If Δ/J is sufficiently large that $c^*\geqslant 1$, then the dc conductivity will vanish for all physically realizable values of c. If $\Lambda=0$, the present model reduces to the quantum percolation problem, which has been the subject of several recent studies [33,52–54]. Our estimate of $c^*\approx 0.5055$ for $\Delta=0$ should be compared with the following numerical estimates of the quantum percolation threshold on a simple cubic lattice: 0.45 [33], 0.38 [52], 0.47 [53] and 0.70 [54]. In the case of dynamic disorder, the critical concentration is

$c^* = I_3(0) \approx 0.5055$, and is independent of J and Δ. In a dynamically disordered system, the carrier moves in a dynamically averaged potential on time scales that are long compared to Λ^{-1}, the correlation time of the fluctuations. Since the critical behavior in this case is determined by dynamics on time scales longer than this correlation time, the critical concentration does not depend on the magnitude of the fluctuations. The critical condition in eq. (7.15a) can be regarded in two ways. One can imagine fixing c and tuning Δ through the transition, or fixing Δ and adjusting c. Fig. 11a shows a phase diagram, calculated from eq. (7.15). To the left of the solid curve, the system is an insulator (zero dc conductivity), and to the right it is a conductor (finite dc conductivity). For $c < I_3(0) \approx 0.5055$, carriers are localized for any value of Δ. For $c > I_3(0)$, carriers are delocalized for $\Delta = 0$, but a transition occurs as Δ is increased. The corresponding phase diagram for nonzero Λ is shown in fig. 11b for comparison. At $c = 1$, there is no topological disorder, and the present model for $\Lambda = 0$ reduces to the model studied in section 6. Since different approximations were used in the derivation of eqs. (7.10) and eqs. (6.3), the predictions of eqs. (7.10) for $\Lambda = 0$ differ in certain respects from those of eq. (6.3). For the original Anderson model, in which the site energies are uniformly distributed between $-W/2$ and $W/2$, the approach of section 6 leads to the prediction that a metal–insulator transition occurs in $d = 3$ at $(W/J)^* = 6.9$, while the present approach yields a prediction of $(W/J)^* \approx 7.5$. In addition, the two approaches yield different predictions for certain of the critical exponents. For example, in eq. (6.9), it is found that the diffusion constant vanishes, as $\chi - \chi^*$, as χ approaches χ^* from above. Eqs. (7.10a)–(7.10d), at $\Lambda = 0$, lead to the prediction that the diffusion constant vanishes as $(\chi - \chi^*)^{1/2}$. A complete discussion of the predictions of eqs. (7.10) at $\Lambda = 0$ is given in ref. [9].

We have analyzed the long time behavior of the transport properties calculated from eqs. (7.10a)–(&.10b), and have elucidated the critical dynamics. Such an asymptotic analysis does not show, however, exactly when this limiting behavior is attained. Estimation of this time is essential in order to determine whether the asymptotic analysis is relevant for a given measurement with a given experimental time scale [61,62]. In order to determine the time regime in which the asymptotic results are valid, one must solve eqs. (710a)–(7.10d). Detailed numerical calculations of $\mathscr{P}_0(t)$ and $\langle r^2(t) \rangle$ were presented in ref. [9]. For $c < c^*$, $\mathscr{P}_0(t)$ approaches a finite value at long times, indicating the carriers are localized in a finite volume. For $c \geq c^*$, $\mathscr{P}_0(t)$ vanishes at long times and the carriers can explore the entire volume. The very long time behavior depends only on c for $\Lambda > 0$ (and $\Delta \neq 0$), but the time scale on which this behavior is first attained depends on Λ and Δ. The time for

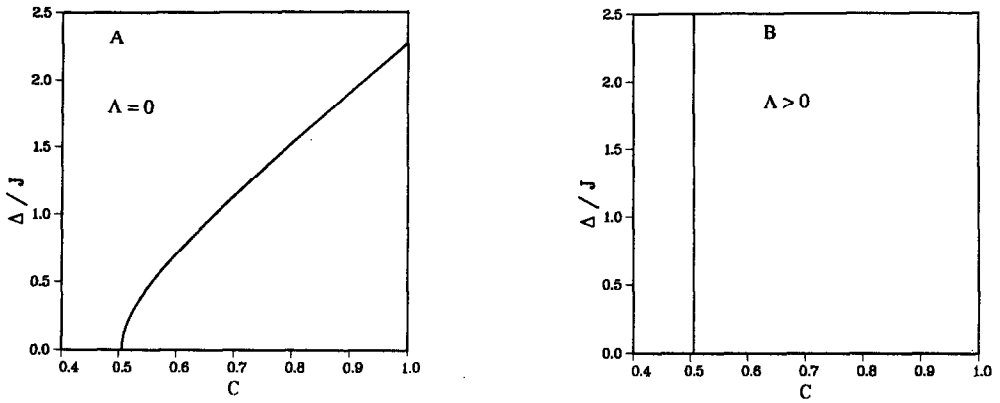

Fig. 11. (a) Phase diagram for a system with topological disorder and static site energy disorder [9]. Δ is the root-mean-squared site energy, J is the intersite interaction, c is the concentration of active sites. To the left of the solid curve, the system is an insulator (zero dc conductivity), and to the right of the solid curve it is a conductor (nonzero dc conductivity). (b) Phase diagram for a system with topological disorder and dynamic site energy disorder [9] characterized by a finite correlation time Λ^{-1}. For $c > c^* \approx 0.5055$, the system is a conductor, and for $c < c^*$ it is an insulator. c^* does not depend on Δ/J, because for times long compared to Λ^{-1}, the carriers move in a dynamically averaged potential.

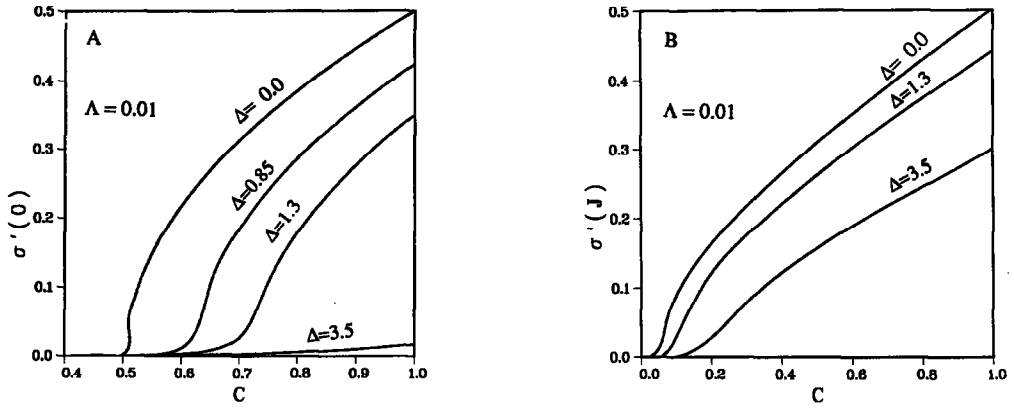

Fig. 12. (a) The concentration dependence of the real part of the dc conductivity is shown for $\Lambda=0.01$ and four values of Δ. The dc conductivity vanishes for $c<c^*$ and is nonzero for $c>c^*$. $c^*\approx 0.5055$. Δ, the root-mean-squared magnitude of the site energy fluctuations, and Λ, the inverse correlation time of the fluctuations are expressed in units of J, the intersite coupling [9]. (b) The concentration dependence of the real part of the ac conductivity evaluated at $\omega=J$ is shown for the same parameters used in A. $\sigma'(J)$ is nonzero for $\Lambda>0$ but still shows an abrupt increase with increasing concentration that resembles a critical point [9].

which the asymptotic behavior holds becomes longer as Λ is decreased or as Δ is increased. For $c>c^*$, $\langle r^2(t)\rangle$ increases linearly with time, whereas for $c<c^*$, it reaches a finite limit at long times and for $c=c^*$, it increases less strongly than linearly in time. In addition, above the critical concentration c^*, $\sigma'(\omega)$ is finite as $\omega\to 0$, while below c^*, $\sigma'(\omega)$ vanishes at $\omega=0$.

In fig. 12a, we display the dc conductivity $\sigma'(0)$ and in fig. 12b, we display the ac conductivity $\sigma'(\omega=J)$ versus the concentration c. $\sigma'(0)$ vanishes for $c<c^*$ whereas $\sigma'(J)$ is always finite. Although $\sigma'(\omega)$ is never zero for $\omega>0$, the curves in fig. 12b display an abrupt increase with concentration which is reminiscent of the critical behavior shown in fig. 12a. Therefore, even for finite frequencies where a critical point does not formally exist, an experimental measurement of the concentration dependence of $\sigma'(\omega)$ would yield a threshold that resembles a metal–insulator transition. Figs. 12a and 12b also demonstrate that the conductivity decreases as Δ increases.

8. Discussion

In this article, we reviewed recent theoretical developments [8–11] which allow the interpretation of spectral lineshapes and quantum transport processes in disordered solids using a unified viewpoint. The key quantity in the present formulation is a frequency-dependent dephasing rate. We first showed how spectral lineshapes of a single molecule in a medium are determined by an intramolecular dephasing rate which controls the relaxation of coherence between the molecular levels. We then introduced the intermolecular dephasing matrix and showed how it determines the spectroscopic and excitation transfer properties of molecular dimers. We then considered the motions of particles or quasiparticles in an infinite medium. The EDA is an analytical approach to treating the localization of a quantum particle moving in a random potential. It is based on the physical intuition that the ensemble averaged density matrix of a particle moving in a random potential satisfies an effective Liouville equation which contains a generalized frequency-dependent dephasing rate $\Gamma(\epsilon)$. The EDA differs from most previous approaches to the quantum localization problem, in that the method focuses on the calculation of the ensemble-averaged density matrix, rather than the averaged wavefunction. $\Gamma(\epsilon)$ describes the loss of phase coherence between different molecules. By transforming to the Wigner representation (eq. (5.4)), we see that $\Gamma(\epsilon)$ can be viewed as a generalized scattering rate in a Boltzmann equation with a BGK collision kernel. The

effective Liouville equation is capable of describing coherent motion ($\Gamma=0$) and incoherent motion (when $\Gamma(0)$ is finite and large compared with the intersite coupling J). The signature of localization is an infrared divergence in $\Gamma(\epsilon)$: $\Gamma(\epsilon)\propto\epsilon^{-\alpha}$. The success of the method in predicting a metal–nonmetal transiton in the Anderson model validates our procedure. The present mapping of the ensemble averaged equation of motion onto an effective Liouville (Boltzmann) equation is ideally suited for treating a broad range of models with static disorder (the Anderson model, quantum percolation) or dynamical disorder (e.g., electron–phonon and electron–electron coupling). It is also ideally suited for developing a semiclassical theory of localization. The applications discussed in this article demonstrate the capacity of the EDA to predict quantitatively the localization transition and all the transport properties, in agreement with scaling theories of localization. The detailed comparisons presented here between the dephasing rate relevant for optical lineshapes and the density of states (eq. (7.9)) and the dephasing relevant for transport (eqs. (7.10) and (7.11)) allow us to analyze the optical and the transport properties in a unified way. We have demonstrated that the dephasing rate associated with transport is much more sensitive to the localization transition than the rate associated with spectral lineshapes.

Acknowledgement

The support of the National Science Foundation, the Office of Naval Research, the US Army Research Office, and the donors of the Petroleum Research Fund, administered by the American Chemical Society, is gratefully acknowledged.

References

[1] N. Bloembergen, E.M. Purcell and R.V. Pound, Phys. Rev. 73 (1948) 679;
P.W. Anderson and P.R. Weiss, Rev. Mod. Phys. 25 (1953) 269;
R. Kubo, Advan. Chem. Phys. 15 (1969) 101.
[2] S. Mukamel, Phys. Rept. 93 (1982) 1; Advan. Chem. Phys. 70 (1988) 165;
S. Mukamel and R.F. Loring, J. Opt. Soc. Am. B 3 (1986) 595.
[3] M. Sparpaglione and S. Mukamel, J. Phys. Chem. 91 (1987) 3938; J. Chem. Phys. 88 (1988) 3267, 4300.
[4] P.W. Anderson, Phys. Rev. 109 (1958) 1492.
[5] R. Abou-Chacra, P.W. Anderson and D.J. Thouless, J. Phys. C 6 (1973) 1734.
[6] P.W. Anderson, Phil. Mag. 52 B (1985) 505.
[7] J.T. de Vreese, ed., Polarons in ionic crystals and polar semiconductors (North-Holland, Amsterdam, 1972).
[8] R.F. Loring and S. Mukamel, Phys. Rev. B 33 (1986) 7708; B 34 (1986) 6582.
[9] R.F. Loring, M. Sparpaglione and S. Mukamel, J. Chem. Phys. 86 (1987) 2249.
[10] R.F. Loring and S. Mukamel, J. Chem. Phys. 85 (1986) 1950.
[11] R.F. Loring, D.S. Franchi and S. Mukamel, Phys. Rev. B 37 (1988) 1874.
[12] S. Mukamel, J. Chem. Phys. 82 (1985) 5398.
[13] J. Sue, Y.-J. Yan and S. Mukamel, J. Chem. Phys. 85 (1986) 462.
[14] Y.-J. Yan and S. Mukamel, 86 (1987) 6085.
[15] S.N. Dixit, P. Zoller and P. Lambropoulos, Phys. Rev. A 21 (1980) 1289;
P. Zoller, G. Alber and R. Salvador, Phys. Rev. A 24 (1981) 398;
H. Risken, The Fokker–Planck equation (Springer, Berlin, 1984).
[16] H. Tsunetsugu, T. Taniguchi and E. Hanamura, Solid State Commun. 52 (1984) 663.
[17] H. Stehfest, Commun. ACM 13 (1970) 47; 13 (1970) 624.
[18] H. Haken and G. Strobl, Z. Physik 262 (1973) 135.
[19] G.H. Hardy, Divergent series (Oxford, 1949).
[20] G. Bergmann, Phys. Rept. 107 (1984) 1.
[21] E. Wigner, Phys. Rev. 40 (1932) 749;
M. Hillery, R.F. O'Connell, M.O. Scully and E.P. Wigner, Phys. Rept. 106 (1984) 121.
[22] H. Mori, I. Oppenheim and J. Ross, in: Studies in statistical mechanics, ed. J. de Boer and G.E. Uhlenbeck (North-Holland, Amsterdam, 1962).

[23] P.L. Bhatnagar, E.P. Gross and M. Krook, Phys. Rev. 94 (1954) 511.
[24] E.N. Economou, Green's functions in quantum physics (Springer, Berlin, 1983).
[25] S. Katsura, T. Morita, S. Inawashiro, T. Horiguchi and Y. Abe, J. Math. Phys. 12 (1971) 892.
[26] G.S. Joyce, Phil. Trans. Roy. Soc. London A 273 (1973) 46.
[27] E. Abrahams, P.W. Anderson, D.C. Licciardello and T.V. Ramakrishnan, Phys. Rev. Letters 42 (1979) 673.
[28] F.J. Wegner, Z. Phys. B 25 (1976) 327.
[29] A. Singh and W.L. MacMillan, J. Phys. C 17 (1985) 2097.
[30] D.C. Licciardello and E.N. Economou, Phys. Rev. B 11 (1975) 3697.
[31] J.L. Pitchard and G. Sarma, J. Phys. C. 14 (1981) L127; 14 (1981) L617.
[32] A MacKinnon and B. Kramer, Phys. Rev. Letters 47 (1981) 1546.
[33] L. Root and J.L. Skinner, Phys. Rev. B 33 (1986) 7738;
L. Root, J.D. Bauer and J.L. Skinner, to be published.
[34] E. Domany and S. Sarker, Phys. Rev. B 20 (1979) 4726;
S. Sarker and E. Domany, Phys. Rev. B 23 (1981) 6018.
[35] D. Vollhardt and P. Wölfle, Phys. Rev. Letters 45 (1980) 842; 48 (1982) 649; Phys. Rev. B 22 (1980) 4666.
[36] Proceedings of the Sixth International Conference on Excess Electrons and Metal–Ammonia Solutions, Colloque Weyl VI, J. Phys. Chem. 88 (1984) 3699.
[37] J. Ludwig, K. Duppen and J. Kommandeur, J. Chem. Soc. Faraday Trans. I 80 (1984) 2943;
I. Rubenstein, M. Bixon and E. Gileadi, J. Phys. Chem. 84 (1980) 715.
[38] G.A. Kenney-Wallace and C.D. Jonah, J. Phys. Chem. 86 (1982) 2572.
[39] C.A. Angell, Solid State Ionics 9 (1983) 3.
[40] S.D. Druger, M.A. Ratner and A. Nitzan, Phys. Rev. B 31 (1985) 3939.
[41] H. Sumi, J. Chem. Phys. 67 (1977) 2943.
[42] A. Blumen and R. Silbey, J. Chem. Phys. 69 (1978) 3589.
[43] K. Kassner and P. Reineker, Z. Physik B 59 (1985) 357; 60 (1985) 87.
[44] R. Silbey and R.W. Munn, J. Chem. Phys. 72 (1980) 2763;
M.K. Grover and R. Silbey, J. Chem. Phys. 53 (1970) 2099.
[45] H. Mueller and P. Thomas, Phys. Rev. Letters 51 (1983) 702.
[46] S.M. Girvin and M. Jonson, Phys. Rev. B 22 (1980) 3583.
[47] T. Holstein, Ann. Phys. NY 8 (1959) 343.
[48] V.M. Kenkre, in: Exciton dynamics in molecular crystals and aggregates, ed. G. Hohler (Springer, Berlin, 1982).
[49] B. Velicky, Phys. Rev. 184 (1969) 614.
[50] R. Parson and R. Kopelman, Chem. Phys. 89 (1984) 265.
[51] S. Abe and Y. Toyozawa, J. Phys. Soc. Japan 50 (1981) 2185.
[52] R. Raghavan, Phys. Rev. B 29 (1984) 748.
[53] V. Srivastava and M. Chaturvedi, Phys. Rev. B 30 (1984) 2238.
[54] T. Odagaki and K.C. Chang, Phys. Rev. B 30 (1984) 1612.
[55] R.F. Loring, H.C. Andersen and M.D. Fayer, J. Chem. Phys. 80 (1984) 5731.
[56] J. Nieuwoudt and S. Mukamel, Phys. Rev. B 30 (1984) 4426.
[57] R.F. Loring, D.S. Franchi and S. Mukamel, J. Chem. Phys. 86 (1987) 1323.
[58] E. Abrahams, P.W. Anderson, D.C. Licciardello and T.V. Ramakrishnan, Phys. Rev. Letters 42 (1979) 673.
[59] S. Chakravarty and A. Schmid, Phys. Rept. 140 (1986) 193.
[60] Y. Gefen, A. Aharony and S. Alexander, Phys. Rev. Letters 50 (1983) 77.
[61] M. Fixman, Phys. Rev. Letters 52 (1984) 791.
[62] S. Havlin, M. Dishon, J. Kiefer and G.H. Weiss, Phys. Rev. Letters 53 (1984) 407.